**UNITED STATES
DEPARTMENT OF COMMERCE**
NATIONAL INSTITUTE OF STANDARDS
AND TECHNOLOGY

NIST Technical Note 1343

Analytical Model for the Refrigeration Power of the Orifice Pulse Tube Refrigerator

Peter J. Storch
Ray Radebaugh
James E. Zimmerman

W
ω

Reservoir
Volume

Piston

Orifice

Heat
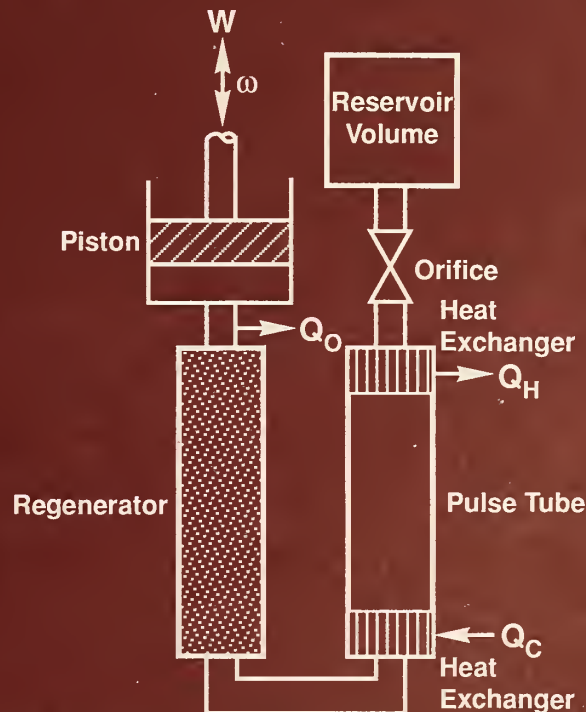Exchanger

Q_O

Q_H

Regenerator

Pulse Tube

Q_C

Heat
Exchanger

Analytical Model for the Refrigeration Power of the Orifice Pulse Tube Refrigerator

Peter J. Storch
Ray Radebaugh
James E. Zimmerman

Chemical Engineering Science Division
Center for Chemical Technology
National Measurement Laboratory
National Institute of Standards and Technology
Boulder, Colorado 80303-3328

U.S. DEPARTMENT OF COMMERCE, Robert A. Mosbacher, Secretary

NATIONAL INSTITUTE OF STANDARDS AND TECHNOLOGY, John W. Lyons, Director

Issued December 1990

NOMENCLATURE

PTR	=	pulse tube refrigerator
BPTR	=	basic pulse tube refrigerator
OPTR	=	orifice pulse tube refrigerator
RPTR	=	resonant pulse tube refrigerator
a	=	slope of average temperature profile
A_g	=	gas cross–sectional area
C_p	=	specific heat of gas
f	=	friction factor
L	=	length of the tube
h	=	specific enthalpy
$\dot{H}$	=	enthalpy flow
$<\dot{H}>$	=	time–averaged enthalpy flow over one cycle
k	=	thermal conductivity
M_t	=	total mass of gas in the table
$\dot{m}$	=	total mass flow rate
$\dot{m}_h$	=	mass flow rate through orifice
$\dot{m}_c$	=	mass flow rate at the cold end
m_{cp}	=	total mass in compressor
$\dot{m}_{cp}$	=	mass flow rate from the compressor
P_d	=	total dynamic pressure
P_a	=	time–averaged pressure
$\dot{Q}_c$	=	heat flow rate into tube at the cold end
$\dot{Q}_h$	=	heat flow rate out of tube at the hot end
R_e	=	Reynolds Number
R	=	gas constant in mass units
r_h	=	hydraulic radius
T_d	=	total dynamic temperature

T_D	=	dead volume temperature (ambient)
T_a	=	time–averaged temperature profile in tube
T_c	=	cold end temperature (x=0)
T_h	=	hot end temperature (x=L, ambient)
T_{cp}	=	compressor temperature (ambient)
T_r	=	reservoir temperature (ambient)
t	=	time
V_{cp}	=	compressor swept volume (total)
V_D	=	dead volume between compressor and pulse tube
V_r	=	volume of reservoir
V_t	=	volume of pulse tube
U	=	total internal energy
u	=	specific internal energy
$\dot{W}$	=	rate of work input
x	=	position along the tube
Z_f	=	flow impedance factor
α	=	phase angle between $\dot{m}_c$ and $\dot{m}_{cp}$
θ	=	phase angle between $\dot{m}_h$ and $\dot{m}_c$
ϕ	=	phase angle between $\dot{m}$ and $\dot{m}_c$
ψ	=	phase angle between T_d and $\dot{m}$
ν	=	linear frequency
ω	=	angular frequency
γ	=	ratio of heat capacities (C_p/C_v)
τ	=	period of one cycle
ρ_a	=	average gas density
η	=	thermodynamic efficiency relative to Carnot
μ_c	=	viscosity at cold end

CONTENTS

Analytical Model for the Refrigeration Power of the
Orifice Pulse Tube Refrigerator

Peter J. Storch, Ray Radebaugh, and James E. Zimmerman

Chemical Engineering Science Division
National Institute of Standards and Technology
Boulder, Colorado 80303

The pulse tube refrigerator is a cryocooler with potential for high reliability. This regenerative refrigerator operates with low average pressures, small compression ratios, and only one moving part. In research conducted at the National Institute of Standards and Technology, a pulse tube refrigerator with an orifice located at the closed, hot end of the system has been used to reach 60 K in one stage. A gross refrigeration power of 12 W has been measured at 80 K with a pulse tube volume of 30 cm³. This paper presents the development of an analytical model to predict the refrigeration power produced in an orifice pulse tube. Three versions of the model are presented: the first calculates quantities which are independent of dead volume; the second neglects dead volume; and the third describes a system with dead volume. Experimental results confirm predictions by the model that refrigeration power is proportional to the average pressure, the pulse frequency, the mass flow ratio, and the square of the dynamic pressure ratio. Results are presented that are useful for approximate design of orifice pulse tube systems. The model assumes adiabatic conditions and an energy balance is performed in terms of net enthalpy flow. Phasor analysis was found to be very useful for analyzing the oscillations of pressure, temperature, and mass flow rate.

Key words: analytical model; cryocooler; cryogenics; pulse tube refrigerator; refrigeration power; refrigerator.

CHAPTER 1

INTRODUCTION

The pulse tube refrigerator (PTR) is a new member of a family of devices known as cryocoolers. Cryocoolers are refrigerators which generate refrigeration at temperatures below 120 K (−244° F) [1]. Pulse tube refrigeration is a cycle of compressions and expansions which pump heat from one end of a tube to the other. Recently, there has been a surge of interest in this method of refrigeration for use in applications which require small, durable cryocoolers. The great advantage of the PTR is its simplicity, which promises to provide high reliability. The lack of reliability in small cryocoolers is a well known problem today.

1.1   Purpose

The general goal of this study is to gain a better understanding of the refrigeration mechanism and the capability of the PTR. More specifically, this work is concerned with developing an analytical model for the refrigeration power generated in an orifice pulse tube refrigerator (OPTR). With the aid of several simplifying assumptions, we derive equations which identify the important parameters in the system. Once the analytical expressions are devised, verification of the model is accomplished by comparing results to previous experimental studies as well as to experiments completed in this work.

A simple, analytical model of the cooling power is useful for three reasons. First, such a model provides insight into the refrigeration mechanism. Often when a numerical model is used to rigorously describe a system, it is difficult to see the physics involved in the process. With an analytical expression, important parameters that affect performance are more easily recognized. Second, basic trends or dependencies of performance can be determined. Such dependencies will aid in optimization and indicate the range of parameters which should be studied in more detail either numerically or experimentally. Third, a simple analytical model will be useful for design. Although not as accurate as a numerical analysis, the model will be convenient for making approximate predictions of system size and refrigeration capacity of the PTR.

1.2   Applications

Cryocoolers including the OPTR have extensive applications today and promise to play an important role in future technology. Presently, cryocoolers can be found cooling infrared detectors to temperatures below 80 K for sophisticated military aircraft, missiles, and tanks. Parametric amplifiers used in ground–based systems for satellite telecommunications and deep–space tracking typically require temperatures below 20 K [2]. The most common commercial application of cryocoolers today is in cryopumping which is important to the semiconductor industry [3]. Cryocoolers have also been tested in space to cool gamma–ray and infrared telescopes [4]. For example, four Stirling refrigerators, developed by a company in cooperation with Johns Hopkins University, flew in space for approximately two years to cool two gamma–ray detectors.

The most important future application for cryocoolers such as the PTR is the cooling of superconductors. It is increasingly apparent that superconducting devices will greatly impact future technology and that cryogenics is the enabling technology. SQUIDs (superconducting quantum interference device) typically require operating temperatures as low as 8 K. However, since 1986 there has been great progress in the development of high temperature superconductors. New copper oxide materials show transition temperatures in excess of 100 K, and may have practical application at 40 or 50 K. Such temperatures are within the range of a two–stage pulse tube refrigerator. SQUIDs are used for making geomagnetic and neuromagnetic measurements and have defense applications in submarine and mine detection. Superconducting magnets at 20 K are used for magnetically suspended, high speed trains, giant particle colliders, energy storage rings, and whole–body magnetic resonance imaging (MRI). In addition, Josephson junctions may define a new generation of digital circuits for high speed computers.

Nowhere is the need for reliability in small cryocoolers more evident than in space applications. Research in cosmic–ray physics, plasma physics, and infrared sensor technology require cryogenic temperatures [5]. Most space missions today are planned to last 3 to 10 years, so a cryocooler in space must operate reliably for a minimum of 3 years to be useful and 5 to 10 years to be considered of real value. Therefore, successful cryogenic designs for space applications require compact and reliable refrigerators with extremely long lifetimes.

1.3   Reliability of the Pulse Tube Refrigerator

The PTR refrigerator has potential for both small size and high reliability. There are two reasons for this potential. First, the pulse tube operates on a regenerative cycle as opposed to a recuperative cycle such as the Joule–Thomson (J–T) refrigerator. In a regenerative refrigerator, the working gas oscillates between the piston at the hot end and the cold end, where cooling is produced.   As gas flows toward the cold end, heat is stored in a unique type of heat exchanger known as a regenerator. Heat is retrieved by the gas as it flows back to the hot end of the tube. Isothermal processes are used for heat addition and rejection. Unlike refrigerators that use recuperative cycles, regenerative refrigerators have neither a J–T valve to become plugged with impurities nor a low–temperature expansion engine with high–pressure seals and valves to wear out. Yasukochi [6] has shown that reciprocating expansion engines account for approximately 25% of failures in recuperative cryocoolers. Regenerative cycles also have the advantages of a simple compressor and a low operating pressure. J–T refrigerators require a valved compressor with compression ratios of up to 200:1 and pressures as high as 20 MPa. The PTR, however, uses only a basic piston without valves and typically operates with a pressure ratio less than 2:1 and an average pressure less than 2.0 MPa. A simpler compressor with lower pressures means less wear, less chance for a leak, and more dependable operation.

The second reason for the potential for high reliability in the PTR is its simplicity. There is only one moving part—the compressor piston at room temperature. The lifetime of mechanical refrigerators can be improved by eliminating moving parts. For instance, the Stirling refrigerator, another regenerative refrigerator, has only two moving parts, and is widely used today. The Stirling refrigerator shown in figure 1–1 operates with a piston at ambient temperature and a displacer between the ambient and cold end temperatures. However, the motion of the displacer generates two problems: the need for seals at low temperatures, which tend to wear, and vibrations close to the refrigeration load, which can decrease the lifetime of the instrument and disrupt the operation of a sensitive detector. The PTR, with no moving parts at low temperature, has potential for longer lifetimes and should be more compatible with sensitive instruments than the Stirling refrigerator.

1.4   Description of the Pulse Tube Refrigerator

Three versions of the pulse tube refrigerator are described in the literature today: 1) the basic pulse tube (BPTR), 2) the orifice pulse tube refrigerator (OPTR), and 3) the resonant pulse tube refrigerator (RPTR). This designation was proposed by Radebaugh
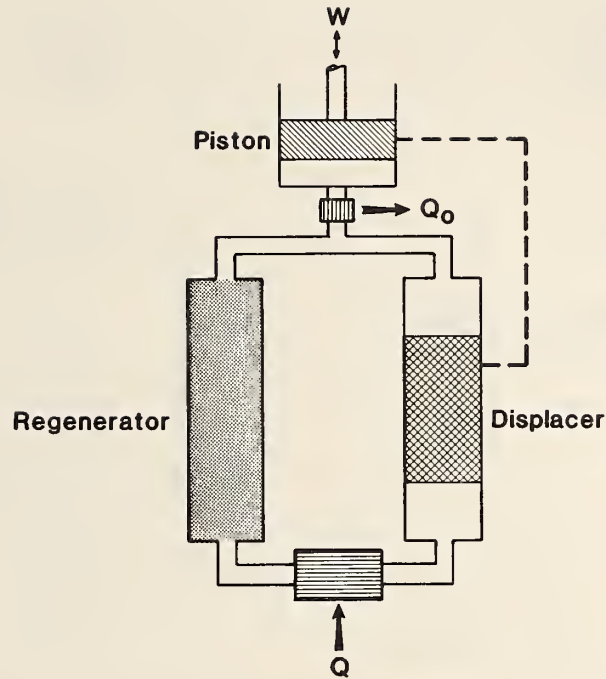
Figure 1–1. Stirling refrigerator.

and coworkers [7] and will be used in this work. The subject of this study is the recently introduced OPTR because of its promise of a refrigeration capacity higher than those of the other two. The components and basic operation of the first two types of PTR are discussed below, while the third is discussed later.

The three primary components of the BPTR, shown in figure 1–2(a), are a piston, a thermal regenerator, and the pulse tube itself. The regenerator is a periodic–flow heat exchanger used to thermally isolate the piston at room temperature and the tube at the cold temperature. The matrix of the regenerator is constructed of material with high heat capacity to absorb heat from and reject heat to the gas as it flows back and forth. The pulse tube is closed at the hot end where a heat exchanger transfers heat from the gas to the surroundings. The tube is open at the cold end to the regenerator and the compressor and has a heat exchanger to transfer heat from the refrigeration load to the gas. The OPTR is shown in figure 1–2(b) with the additional components of an adjustable orifice and the reservoir volume.
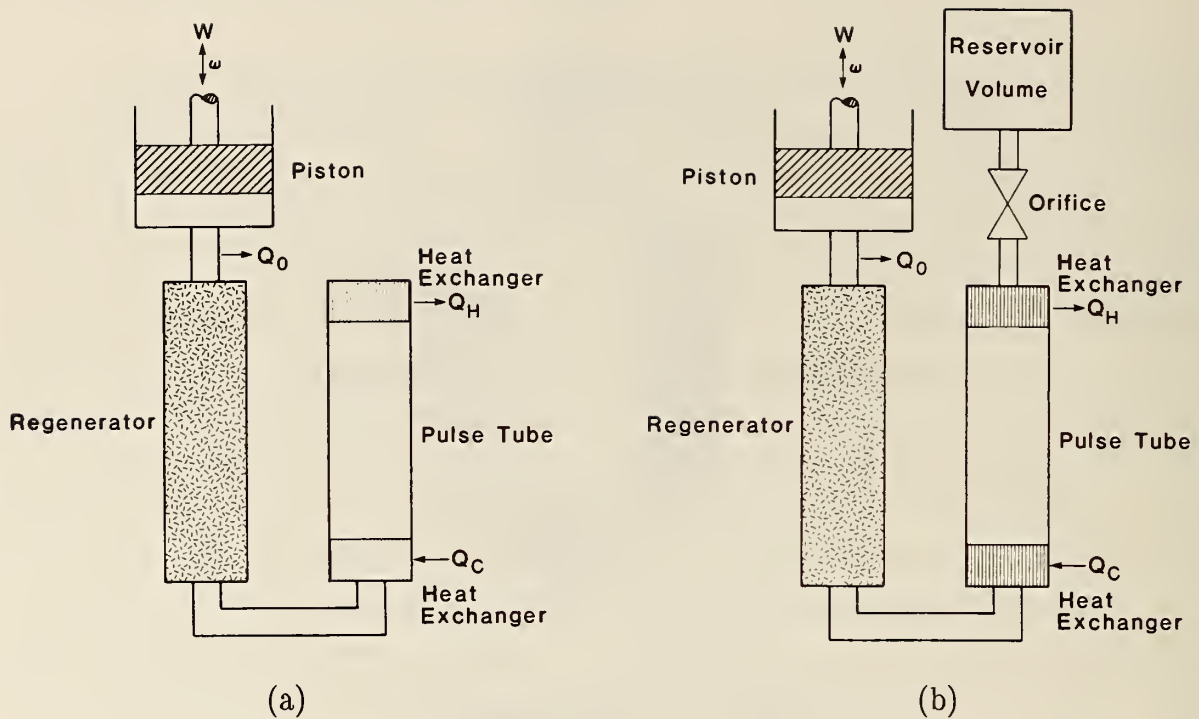
Figure 1–2.   (a) Basic pulse tube refrigerator
    (b) Orifice pulse tube refrigerator

The refrigeration cycle for both types of the PTR is best understood by examining the temperature–position history of a single element of gas in the BPTR. Figure 1–3 shows the temperature of a gas element as a function of position in the tube. The first half of the cycle begins when the piston moves gas into the tube. The gas is cooled to the temperature of the cold end (point 1) as it flows through the regenerator. The element of gas in the tube is compressed adiabatically and is heated as it travels toward the closed end (point 1 to point 2). Constant–volume cooling then occurs during a relaxation period at high pressure (point 2 to point 3). During this period, heat is rejected in the hot–end exchanger while the gas element in the tube is cooled by transferring heat with the tube wall. The second half of the cycle occurs as the piston moves gas from the tube back through the regenerator. An element in the tube is expanded adiabatically and cools as it moves toward the open end (point 3 to point 4). The cycle is completed with a relaxation period of constant–volume heating at low pressure (point 4 to point 1). Gas in the
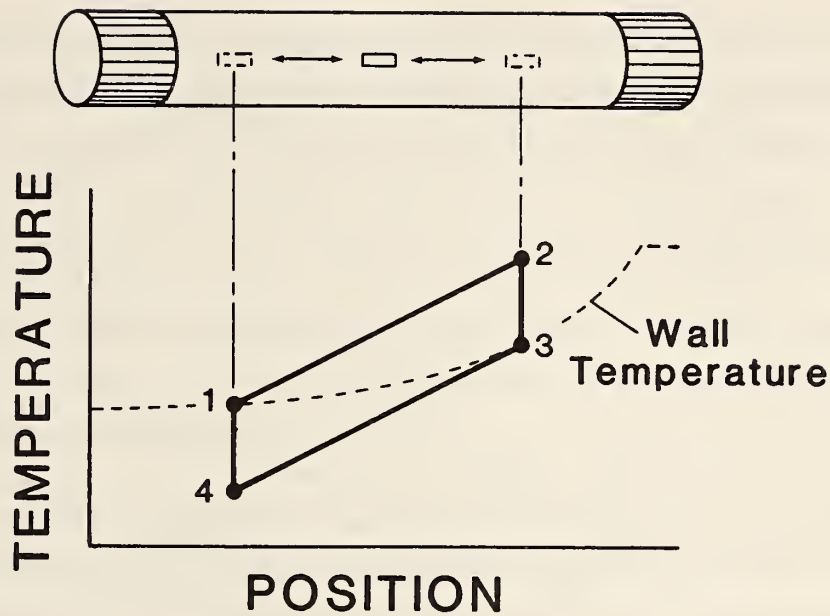
Figure 1–3.   Temperature as a function of position for an element of gas in
the basic pulse tube refrigerator.

cold–end heat exchanger absorbs heat from the load while gas in the tube is heated by the
wall. The consequence of operating a system on this cycle is a net flow of enthalpy or
pumping of heat from the cold end to the hot end. A constant temperature gradient in the
tube is established, and continuous refrigeration is produced.

The OPTR follows the same refrigeration cycle as described above except for the
method of heating and cooling during the relaxation periods. Instead of exchanging heat
with the tube wall, an element of gas in the OPTR experiences a change in temperature
due to flow through the orifice. As gas flows from the tube through the orifice and into the
reservoir, gas remaining in the tube expands adiabatically and cools. As gas flows back
into the tube from the reservoir, gas in the tube is adiabatically compressed and heats up.

1.5   AC Circuit Analogy

The oscillating behavior of flow in pulse tube systems is reminiscent of a common
AC electrical circuit. In fact, each mechanical component and action in the PTR has an
electrical counterpart. For instance, the flow of electrons or current in an electrical circuit
is analogous to the mass flow of the fluid in the pulse tube, while voltage is analogous to

pressure.   A voltage drop occurs from resistance in a circuit just as a pressure drop occurs from anything that impedes flow in the PTR. Also, a capacitor, which stores charge, can be used to represent a volume which stores mass in the PTR system.

The analogous circuit is shown in figure 1–4. The AC voltage source (element 1) produces a sinusoidal voltage and current in the electrical system in much the same way the compressor produces sinusoidal pressure and mass flow oscillations in the pulse tube. However, for large pressure oscillations, there is significant deviation from sinusoidal behavior and the compressor behaves more like a variable capacitor. Current from the voltage source flows through the first resistor (element 2), which represents the solid matrix in the regenerator, and a drop in voltage or pressure occurs. At this point, current is diverted in the circuit to charge a capacitor (element 3), just as part of the mass flow from the compressor is required to pressurize the regenerator void volume. The resulting current then encounters the next two resistor–capacitor sets (elements 4, 5 and elements 6, 7), which represent dead volume and pulse tube volume with similar effect. Each volume in the pulse tube can be associated with a resistance and a capacitance in the circuit. The last resistor in the circuit (element 8) models the flow impedance of the orifice at the hot end of the pulse tube. Again, a drop in voltage or pressure occurs here as charge or mass flows into the large capacitor (element 9) representing the reservoir volume.

Drawing the analogy between the pulse tube and a familiar system such as a basic AC circuit can help us better understand the function of components in a PTR. The
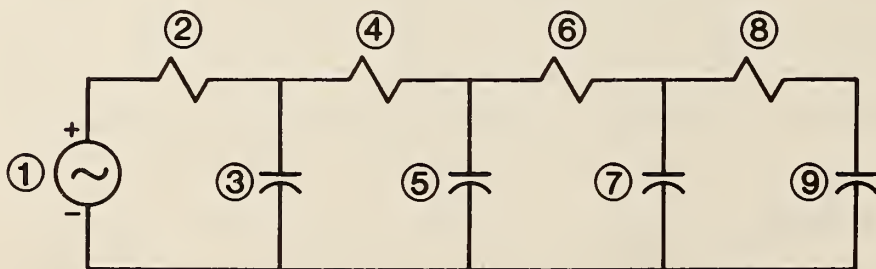

Figure 1–4. Analogous A C circuit for the orifice pulse tube refrigerator.

electrical model is also useful because methods for analyzing such systems are well established. Specifically, phasor analysis and complex algebra, which are commonly used to study AC circuits, can be applied effectively to PTR systems. Also associated with sinusoidal voltage and current are phase angles; and it becomes very convenient to describe oscillations in mass flow rate, pressure, and temperature with phase relationships.

1.6 History of Pulse Tube Refrigeration Research

1.6a Thermal Acoustic Oscillations

Heat pumping found in the PTR is closely related to another phenomenon known as thermal acoustic oscillations. Such oscillations occur spontaneously in tubes with a large temperature gradient between a closed hot end and an open cold end, and they are commonly encountered today in the storage and transfer of cryogens. Successful theoretical models for helium were presented by Rott in 1969 [8] and 1973 [9]. One of the earliest and most well known observations of thermal acoustic oscillations was made by C. Sondhauss in 1850. He noticed a sound produced from tubes used by glass blowers. When a gas flame was applied to a glass bulb at the end of a tube open to the room, air in the tube oscillated producing a sound characteristic of the tube dimensions. Lord Rayleigh in 1878 offered an explanation for this spontaneous occurrence by pointing out that oscillations occur if heat is added to the air at the point of highest pressure and removed at the point of lowest pressure [10]. In other words, energy in the form of heat is introduced at the closed end and energy in the form of acoustic waves and heat is removed at the open end. This phenomenon is simply the reverse of the process in the PTR where energy is introduced at the open end in the form of pressure waves and removed at the closed end as heat to provide useful refrigeration.

1.6b The Basic Pulse Tube Refrigerator

The use of thermal acoustic phenomena to generate refrigeration was first proposed by Gifford and McMahon in 1959 [11]. The first pulse tube refrigerator apparatus, along with a theory of the refrigeration process, was described in detail by Gifford and Longsworth in 1964 [12]. This early PTR was similar to the device described above and shown in figure 1–2. Gifford and Longsworth concluded that only those elements of gas traveling between the hot– and cold–end heat exchangers were responsible for the refrigeration effect. This idea was later refuted by the same authors in a second paper

written in 1965 [13]. Gifford and Longsworth found that the PTR still operated below the critical pressure ratio where gas does not make the complete passage between the heat exchangers. A third paper entitled "Surface Heat Pumping" was published a year later, giving a much better qualitative description of the refrigeration effect [14]. The main points of this description have been reviewed in the explanation of the BPTR noted earlier.

All experiments up to this point had been performed on PTR systems that used valved compressors to generate the pressure wave. Longsworth used such a valved PTR in 1967 to reach a low temperature of 124 K with no load [15]. He measured a gross refrigeration of 5 W at this temperature, which was totally absorbed by inefficiencies such as regenerator ineffectiveness and conductive losses. That same year, Gifford and Kyanka reached 165 K using a reversible PTR, that is, a PTR with a piston compressor instead of a valved system [16]. The idea of using a piston as a driver was first mentioned by Gifford and Longsworth in 1965 as a method of overcoming the large inefficiency introduced by irreversible expansion through the pressurization valves. Gifford and Kyanka showed that the reversible system had a work requirement of only 10% of that of an ideal valved system. However, the refrigeration capacity of the reversible PTR was shown to be much less than the valved PTR at low pulse frequencies. This is due to the fact that a piston generates pressure oscillations that are approximately sinusoidal. A valved system, however, generates more of a "square wave" oscillation, which provides more time for heat transfer between the gas and the wall. Gifford and Kyanka pointed out that performance of the reversible PTR increases with frequency and should have been comparable to that of the valved system at higher frequencies.

Although work on the BPTR was certainly interesting and gave valuable insight into the mechanism of refrigeration, the lowest temperatures achieved were still too high to be of practical use. Most applications of cryocoolers are below 80 K. Therefore, interest in pulse tube refrigeration diminished and no great progress was made until recently when some new concepts were introduced.

1.6c The Resonant Pulse Tube Refrigerator

A new idea in pulse tube refrigeration was presented by Merkli and Thomann in 1975 [17]. They showed in principle that a tube closed at one end and filled with gas oscillating at a resonance frequency could be used as a heat pump. They measured cooling in the section of the tube with maximum velocity (pressure node) and heating in the region

of the velocity nodes (pressure antinodes). However, the refrigeration produced in the tube was minimal. Then, in 1983 and 1985, Wheatley and coworkers published two papers in which they described a resonant tube having an internal structure of plates [18] [19]. This structure or "stack" of plates becomes a second thermodynamic medium (the first is the working fluid) in which a net enthalpy flow is generated. A basic schematic of RPTR is shown in figure 1–5. The system consists of an acoustic driver at the open end of the tube, the resonance tube with the second thermodynamic medium, and a gas spring at the closed end. A regenerator is not required with this configuration because the hot end of the plates is toward the driver. In one case, a stack of cloth–epoxy plates was used in the tube, and a low temperature of 195 K was measured at a frequency of 516 Hz and an average pressure of 1 MPa. The most recent work on resonant pulse tubes or thermoacoustic refrigerators has been done by Tom Hofler in 1986. His apparatus uses a polymer film roll structure in the resonator. With the hot end at 300 K, this device reached a cold end temperature of 200 K. An efficiency equal to 18% of Carnot efficiency was obtained.

1.6d The Orifice Pulse Tube Refrigerator

The second major innovation for the PTR came in 1984 when the Russian scientist E.I. Mikulin inserted an orifice at the closed end of the tube [20–22]. He called this an "expansion" pulse tube because the orifice allows part of the gas to expand into a large reservoir. The effect of the orifice on the refrigeration mechanism was a large increase in the refrigeration capacity. Originally, Mikulin placed the orifice between the hot tube and the heat exchanger at the hot end and used a valved compressor with air as the working fluid. With a pressure ratio (P_{max}/P_{min}) of 2, a frequency of 15 Hz, and no thermal load, a
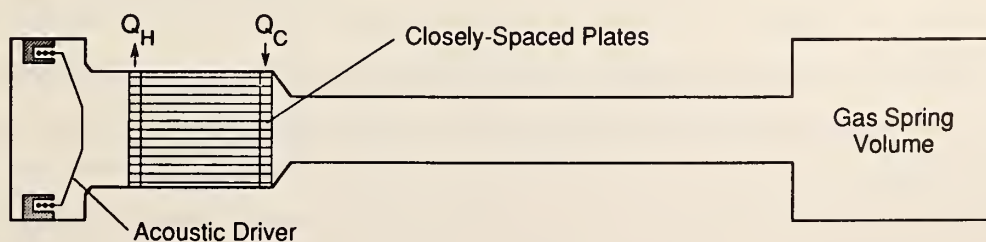

Figure 1–5. Resonant pulse tube refrigerator.

temperature of 105 K was achieved and 10 W of refrigeration were measured at 120 K. The pulse tube in this case had a volume of 35.3 cm³. However, the paper does not provide details as to the amount of gas that was leaving and entering the pulse tube through the orifice during one cycle.

In 1985, Radebaugh and coworkers at the NIST, formerly the National Bureau of Standards (NBS), modified Mikulin's configuration slightly and relocated the orifice on top of the hot end heat exchanger [8]. This configuration has been designated as the orifice pulse tube refrigerator and is the same apparatus used in this work as shown in figure 1–2b. Radebaugh's version uses a piston compressor with helium as the working fluid. For a 30 cm³ pulse tube, after optimizing the orifice setting a gross refrigeration capacity of 18 W was measured. This measurement was taken at the low temperature of 60 K with P_{max} = 1.24 MPa, P_{min} = 0.71 MPa, and a frequency of 9 Hz. The mass flow rate through the orifice was calculated to be about 50% of the flow rate at the cold end. The point was made that frequency and pressure ratio were not totally optimized for these measurements. Also, with improved regenerators and multiple stages, Radebaugh indicated it may be possible to reach a temperature of 10 K [8].

Experimental work on the OPTR at NIST has continued and some very useful results were published in 1986 by Radebaugh and Herrmann [23] [24]. Many important conclusions about the operation and performance of the OPTR were presented. Measurements of efficiency and refrigeration capacity were made with four different pulse tube sizes. Measurements were taken with helium gas at an average pressure of 1 MPa and a pressure ratio (P_{max}/P_{min}) of 2.6. The best performance was obtained with a 30 cm³ tube at a frequency of 6 Hz, generating 15 W of refrigeration power at 100 K. The intrinsic thermodynamic efficiency measured for this case was 40% of Carnot efficiency at the optimum orifice setting which occurred when the ratio of mass flow through the orifice to mass flow in the tube ($\dot{m}_h/\dot{m}_c$) was 0.35. The thermodynamic efficiency was defined using the P–V work in the tube (see eq (3–8)). The data supported the idea that efficiency decreases with an increase in flow through the orifice. Radebaugh and Herrmann also showed that, although the thermodynamic efficiency of the BPTR (orifice closed) was generally twice as high as for the OPTR, the refrigeration power produced with the orifice was as much as 10 times greater than the BPTR. The fact that the OPTR has a lower thermodynamic efficiency and a larger refrigeration power than the BPTR indicates the presence of a different mechanism for pumping heat. Radebaugh and Herrmann also point out that efficiency of the OPTR is comparable to that of the Stirling refrigerator and

12

greater than that of the Joule–Thomson refrigerator [24]. Finally, another important conclusion from this work was that refrigeration capacity depends on volume and not on length or diameter of the tube, although there is certainly a minimum limit on these parameters.

CHAPTER 2

ANALYTICAL MODEL

Since the OPTR was first introduced in the late 1970's by Tarasov and Mikulin, only one analytical expression describing the refrigeration power has been published. This expression was first presented by Mikulin and coworkers in the Soviet Union in two papers in 1982 and 1983 [20], [21], and then in the United States in 1984 [23]. Mikulin developed an adiabatic model for the tube assuming ideal heat exchange and the absence of friction. Three equations were presented for the average expanded gas temperature, the refrigeration power, and the thermodynamic efficiency [22]. Unfortunately, it is not clear how the model demonstrates the effect of flow through the orifice on the refrigeration power.

Like Mikulin's model, the analysis presented in this paper treats the ideal case of an adiabatic tube. Support for the idea that processes in the orifice pulse tube are actually adiabatic is found in experiments by Radebaugh and Herrmann which show that heat transfer between the fluid and the tube wall actually decreases the performance [24]. However, in this case, the idea of enthalpy flow is used to describe the system. This model also attempts to show the role of the orifice in the refrigeration mechanism, which has already been established experimentally as an important factor in performance [23].

2.1   Enthalpy Flow Analysis

In the past, a typical method of analyzing regenerative type refrigerators has been to assume isothermal compression and expansion so that the heat transferred in one cycle is equal to the P–V work done. The most obvious example of this method is the Schmidt analysis used to model Stirling refrigerators [1, p.134]. Adiabatic modeling has also been applied to Stirling engines, for example, by Finklestein with very useful results [1, p.142]. Unfortunately, such adiabatic models have not produced closed–form solutions, which is the goal of this work.

In 1985, Radebaugh took a new approach to regenerative systems when he employed an enthalpy–flow analysis to compare three types of PTRs [8]. This is the same simple, but powerful, method commonly used in the analysis of steady–flow, recuperative systems such as the Joule–Thomson refrigerator. The study of enthalpy flow in a regenerative system is more complicated due to the oscillating flow. Temperature, pressure, and mass flow rate are functions of time and position in real systems. However, the advantages of an enthalpy–flow analysis are that it eliminates work terms in the energy balance and creates simple boundary conditions. P–V work is included in the definition of enthalpy: $H = U + PV$ where U is internal energy. The system described by the model and to be analyzed for enthalpy flow is that shown in figure 2–1. It is emphasized that this work does not attempt to model the entire pulse tube system with the compressor and regenerator. Rather, the system of interest here consists only of the tube, which is assumed to be completely adiabatic, and the hot– and cold–end heat exchangers, which are assumed to be ideal and isothermal.

Figure 2–1 presents the heat flows to be considered in the energy balance: $<\dot{H}>$ is the net enthalpy flow, $\dot{Q}_c$ is the rate of heat flow in at the cold end, or the refrigeration effect, and $\dot{Q}_h$ is the rate of heat flow out of the hot end. $<\dot{H}_r>$ is more appropriately defined later.
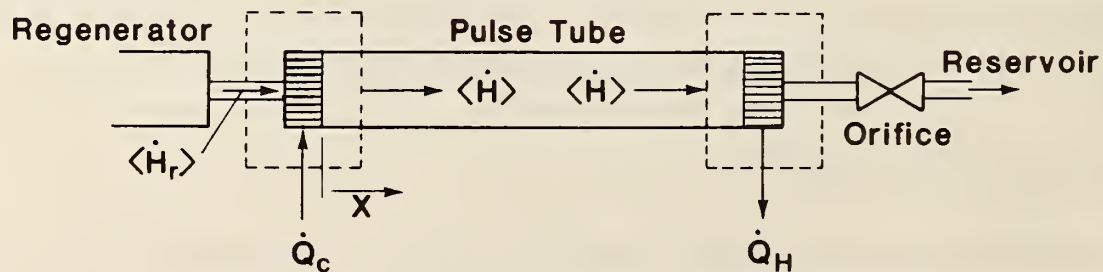

Figure 2–1.   The OPTR system described by the model. Net heat flows considered in energy balance are displayed.

The energy balance for figure 2–1 begins with the first law of thermodynamics for a steady–flow, open system,

$$\dot{Q} = \dot{W} + \dot{m}(h_{out} - h_{in}), \tag{2–1}$$

where $\dot{Q}$ is the refrigeration power, $\dot{W}$ is the rate of work produced by the fluid, $\dot{m}$ is the mass flow rate in the tube, and h is the specific enthalpy of the fluid at the inlet or outlet. We define enthalpy flow as

$$\dot{H} = \dot{m}h. \tag{2–2}$$

For a pulse tube refrigerator with oscillating flow, the energy balance is

$$<\dot{Q}> = <\dot{W}> + \Delta<\dot{H}>, \tag{2–3}$$

where all energy flows are averaged over one period of oscillation.

First consider the cold end of the system, shown on the left half of figure 2–1. Because the system boundaries do not change (constant tube volume) and the P–V work is accounted for in the enthalpy term, the work flow $\dot{W}$ is 0. The rate of heat flow into the cold end then is equal to the change in the enthalpy flow,

$$\dot{Q}c = \Delta<\dot{H}> = <\dot{H}> - <\dot{H}_r>. \tag{2–4}$$

The term $<\dot{H}_r>$ is the average enthalpy flow into the system from the regenerator due to regenerator ineffectiveness, conduction in the regenerator matrix and tube wall, and other loss terms. Therefore, $\dot{Q}_c$ represents the net refrigeration power available, while the enthalpy flow in the tube $<\dot{H}>$ is the gross refrigeration power.

The energy balance is then likewise applied to the hot end of the system in figure 2–1. Because flow through the orifice is assumed to be isothermal, the net enthalpy flow over one cycle for the gas leaving and entering the tube is zero. Therefore, the rate at which heat is rejected at the hot end is simply equal to the enthalpy flow in the tube or the gross refrigeration power,

$$\dot{Q}_h = <\dot{H}>. \tag{2–5}$$

The energy balances in eqs (2–4) and (2–5) reveal three interesting points about the PTR. First, a unique property of this refrigerator is that the gross refrigeration and the net refrigeration can be measured simultaneously. Second, if loss terms are negligible, $\dot{Q}_c = \dot{Q}_h$, and the available refrigeration power can be measured at either end of the tube. It is important to remember that the statement $\dot{Q}_c = \dot{Q}_h$ represents only an energy balance on the tube and not the entire refrigeration system. An overall balance would include the heat rejected at the compressor. Third, given the ideal, adiabatic tube, there is no addition of heat at any point in this region and the enthalpy flow must be constant.

The energy balances also show that the gross refrigeration power in the orifice pulse tube can be modeled by developing an equation for the net enthalpy flow $<\dot{H}>$; this is now the task ahead.

The derivation begins with the equation

$$dh = \left[\frac{\partial h}{\partial T}\right]_P dT + \left[\frac{\partial h}{\partial P}\right]_T dP, \tag{2–6}$$

which shows the change in enthalpy as a function of T and P. For an ideal gas with specific heat capacity at constant pressure C_P, it is a standard result of thermodynamic theory that

16

$$\left[\frac{\partial h}{\partial P}\right]_T = 0 \quad \text{and} \quad \left[\frac{\partial h}{\partial T}\right]_P = C_P = \text{constant.} \tag{2-7}$$

Using these results, integration of eq (2–6) gives

$$h = h(T_o) + C_P (T-T_o), \tag{2-8}$$

where T_o is some reference temperature. T_o in this case is assigned to be the average temperature T_a of the gas at any point in the tube. The instantaneous temperature is defined to be

$$T(x,t) = T_a(x) + T_d(x,t). \tag{2-9}$$

T_d is called the dynamic temperature, which is the amplitude of the temperature oscillation and is a function of time and position. Therefore, specific enthalpy in eq (2–8) becomes

$$h = h(T_a) + C_P T_d. \tag{2-10}$$

Then multiplying all terms by $\dot{m}$ and using the definition of enthalpy flow,

$$\dot{H} = \dot{H}(T_a) + \dot{m}C_P T_d. \tag{2-11}$$

Integration over one cycle of period τ gives the average or net enthalpy flow. Because the first term in eq (2–11) integrates to zero,

$$<\dot{H}> = (C_P/\tau) \int_0^\tau \dot{m}T_d \, dt. \tag{2–12}$$

Thus far, it has been established for the ideal system that the average enthalpy flow depends on the oscillations of mass flow rate and temperature, as shown by eq (2–12). Both of these oscillations are assumed to be sinusiodal in time, and both are functions of position along the tube. However, in order to satisfy the law of conservation of energy, the average enthalpy flow along the adiabatic tube must be constant. An important test for thermodynamic consistency in the model will be the cancellation of the postion dependency in the product of $\dot{m}$ and T_d.

2.2   Phasor Analysis

Equation (2–12) is a general expression for the average enthalpy flow in the OPTR for an ideal gas. It shows that $<\dot{H}>$ depends on the interaction between the mass flow rate and the dynamic temperature oscillations. Flow through the orifice affects the forms of these oscillations and their interaction. Therefore, it is difficult to visualize and model such oscillatory behavior without some simplifications.

The first step taken in describing the oscillations in the OPTR is to assume that the pressure oscillation is sinusoidal in shape, which means the mass flow rate and temperature oscillations also behave as sinusoids. This assumption is good for small ratios of dynamic pressure to average pressure ($P_d/P_a \ll 1$) and greatly simplifies the mathematics involved in the analysis. The second step taken to help visualize the interaction of the oscillations of pressure, temperature, and mass flow rate is to represent the sinusoids as phasors. Phasor analysis is commonly used to study currents and voltages in AC electrical networks [25]. A phasor is a vector operating in "phase space" instead of in physical space. It has magnitude and direction corresponding to the amplitude and phase angle of a sinusoid. The phasor operates in the frequency domain and rotates at an angular velocity corresponding to the angular frequency of the sine oscillation in the time domain. The right side of figure 2–2 shows phasor $\underline{A}$ with magnitude $|A|$ and angle θ. As time progresses, the phasor rotates counter–clockwise and traces out the amplitude of the sine oscillation on the left side of the figure. Since all the oscillations in the pulse tube have the same frequency, their phasors will have the same angular velocity and maintain their relative positions in the frequency domain. These vectors can then be manipulated by the
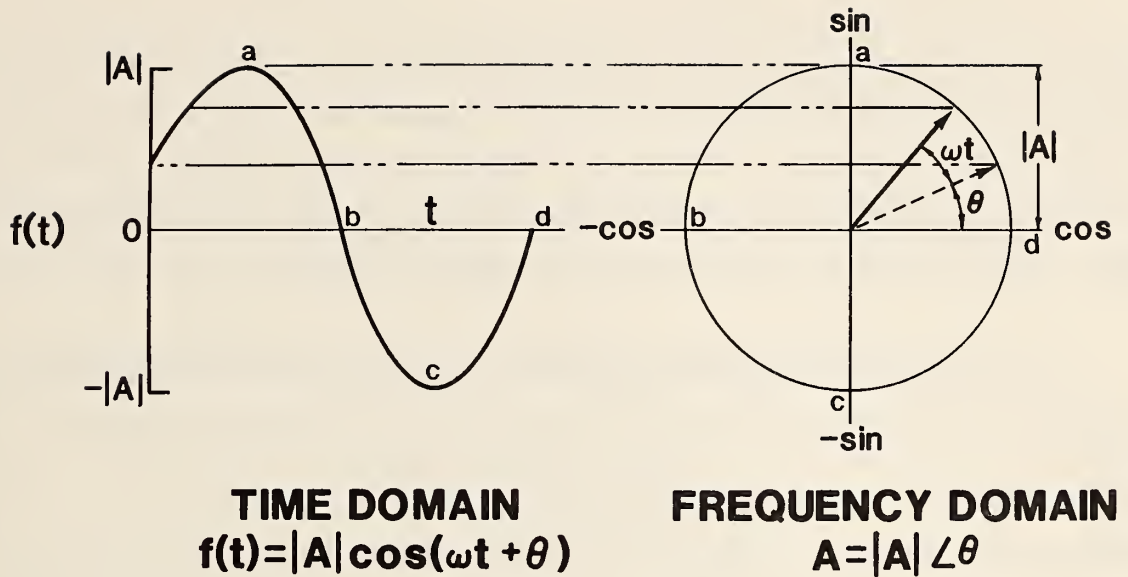
TIME DOMAIN
$$f(t) = |A|\cos(\omega t + \theta)$$

FREQUENCY DOMAIN
$$A = |A| \angle \theta$$

Figure 2–2. Sine oscillation f(t) is produced in the time domain by rotating phasor A in the frequency domain.

ordinary rules of vector geometry. A phase angle does not affect the form of the oscillation, but only fixes the origin in time.

2.3   Phase Angles

Phase angles are used to describe the phase relationship between the various oscillations in the pulse tube. According to eq (2–12), the average enthalpy flow is determined by integrating the product of $\dot{m}$ and T_d over one cycle. If these quantities are written in terms of sinusoids, the integral has the form,

$$I = \int \sin \omega t \, \sin(\omega t - \psi) dt, \qquad (2\text{–}13)$$

where ψ is the phase angle between the functions describing $\dot{m}$ and T_d. Integrating eq (2–13) over one cycle and dividing by τ results in the following term:

19

$$I = \tfrac{1}{2} \cos \psi. \qquad\qquad (2\text{--}14)$$

Since $<\dot{H}>$ is proportional to I, $<\dot{H}>$ is a maximum when $\psi = 0$ and $\dot{m}$ and T_d are in phase. Similarly, $<\dot{H}> = 0$ when $\dot{m}$ and T_d are 90° out of phase.

In a physical sense, the angle ψ represents the relative time difference between the occurrence of a flow rate maximum and the occurrence of a temperature maximum. ψ is affected then by the relaxation periods of cooling and heating in the pulse tube. A shift in phase in the BPTR takes place when the gas exchanges heat with the tube wall. In the OPTR, a phase shift occurs when gas in the tube is expanded or compressed due to flow through the orifice. Since the phase angle is an important parameter for enthalpy flow, it is expected that the method of phase shift will produce a difference in performance between the two pulse tubes. (See <u>Describing the Refrigeration Process</u> in chapter 4.)

2.4   Mass Flow Rate Equation

The development of an expression for the mass flow rate involves an energy balance on the tube as shown in figure 2–3.
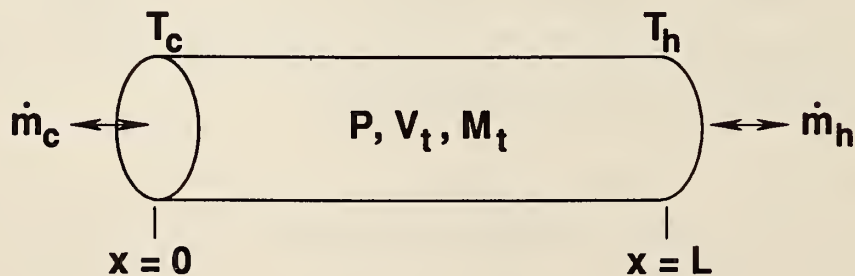

Figure 2–3.   Adiabatic pulse tube system with mass flows $\dot{m}_c$ at the cold end and $\dot{m}_h$ at the hot end.

The system we attempt to model consists of an adiabatic tube with constant volume V_t, pressure P, and a total mass of gas M_t. The mass moving in and out at the ends of the tube $\dot{m}_c$ and $\dot{m}_h$, maintain constant temperatures T_c and T_h. We assume no mixing of the moving gas elements with bulk gas in the tube, which means the only effect of these mass flows in the model is to change the pressure.

The energy balance for an open system with non-steady flow is

$$\frac{dU}{dt} = \dot{Q} - \dot{W} - \Delta \dot{H}, \tag{2--15}$$

where U is the total internal energy. For the tube with constant boundaries without heat transfer between the gas and the tube wall, $\dot{W} = 0$ and $\dot{Q} = 0$. The energy balance then becomes:

$$\frac{d(\rho V u)}{dt} + \dot{m}_h h_h - \dot{m}_c h_c = 0, \tag{2--16}$$

where ρ is the gas density, V is the system volume, u is the specific internal energy, and h_h and h_c are the specific enthalpies of the gas at the hot- and cold-end temperatures respectively. Assuming an ideal gas,

$$u = C_v T = C_v \frac{P}{\rho R}, \tag{2--17}$$

$$h_h = C_P T_h, \tag{2--18a}$$

and

$$h_c = C_P T_c. \tag{2--18b}$$

After substituting eqs (2–17) and (2–18) into the energy balance, and using V_t for the general system volume, the energy balance becomes

$$\frac{C_v V_t}{C_p R} \frac{dP}{dt} = \dot{m}_h T_h - \dot{m}_c T_c.$$

(2–19)

Defining γ as the ratio of heat capacities C_p/C_v and rearranging eq (2–19) gives the result,

$$\frac{V_t}{\gamma R T_c} \frac{dP}{dt} = \dot{m}_h \frac{T_h}{T_c} - \dot{m}_c.$$

(2–20)

The left side of this equation represents the change in mass in the tube $\frac{dM_t}{dt}$ due to mass flow in and out at the tube ends. Because of the temperature gradient along the tube and the assumption of no mixing between the working fluid entering and leaving the tube and the bulk of the fluid in the adiabatic tube, the total change of mass is written in terms of the cold end temperature. Integrating the equation

$$\frac{dM_t}{dt} = \frac{V_t}{\gamma R T_c} \frac{dP}{dt}$$

would not give the true total mass because it was assumed that mixing does not occur in the tube. T_h/T_c accounts for the effect of mass leaving or entering the tube at different temperatures. The final result is

$$\frac{dM_t}{dt} = \dot{m}_h \frac{T_h}{T_c} - \dot{m}_c.$$

(2–21)

In terms of phasors the mass balance becomes

$$\frac{dM_t}{dt} = \dot{\underline{M}}_h \frac{T_h}{T_c} - \dot{\underline{M}}_c. \qquad (2\text{--}22)$$

In order to avoid confusion in the representations of the oscillations of mass flow rate, pressure, and temperature, phasors are represented by underlined upper case letters, amplitudes are shown in just upper case letters, and functions in the time domain are written in lower case letters. The phasor diagram depicting mass flow rates in the orifice pulse tube is shown in figure 2–4.

The phasor $\dot{\underline{M}}_c$ is taken as the reference phasor and assigned the value cos ωt. All other phasors, in terms of phase angle, are described in relation to this $\dot{\underline{M}}_c$. For example, θ is the phase angle by which mass flow through the orifice $\dot{\underline{M}}_h$ lags the mass flow at the cold end $\dot{\underline{M}}_c$.
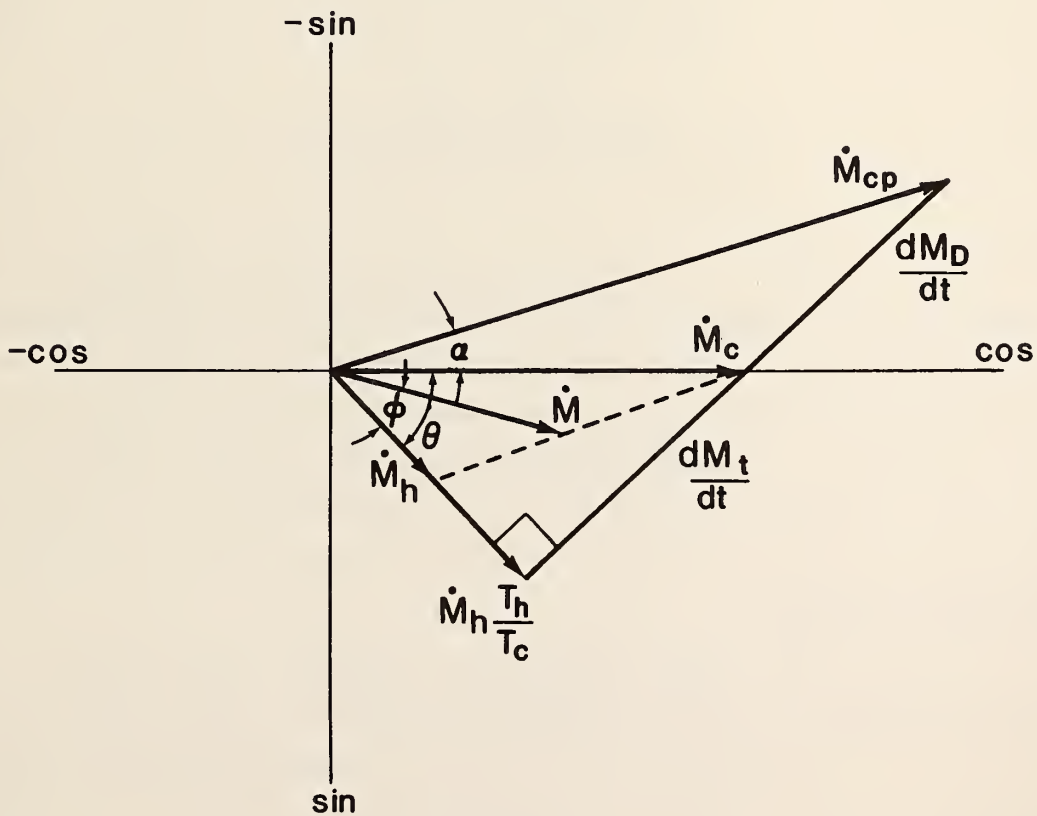
Figure 2–4. Phasor diagram of mass flow rate in the orifice pulse tube.

23

The angle θ is also the phase shift between $\underline{P}_d$ and $\underline{\dot{M}}_c$ because laminar flow through the orifice is proportional to the dynamic pressure. The sinusoid for the dynamic pressure is written simply as

$$p_d(t) = P_d \cos(\omega t - \theta). \qquad (2\text{--}23)$$

Pressure drop in the pulse tube is neglected and pressure is therefore a function of time but not of position.

The angle between $\underline{\dot{M}}_h(T_h/T_c)$ and $d\underline{M}_t/dt$ must be 90°, so $d\underline{M}_t/dt$ is proportional to the pressure derivative dP/dt, as shown in eq (2–20). Figure 2–4 then gives an important trigonometric relationship for phase angle θ:

$$\cos\theta = (\dot{M}_h/\dot{M}_c)(T_h/T_c), \qquad (2\text{--}24a)$$

or
$$\sin\theta = \sqrt{1 - (\dot{M}_h/\dot{M}_c)^2(T_h/T_c)^2}\,. \qquad (2\text{--}24b)$$

Another important feature of the phasor diagram in figure 2–4 is the total mass flow rate, $\underline{\dot{M}}$. Mass flow rate in the tube is a function of temperature and pressure and therefore depends on time and position in the tube. Total mass flow rate $\dot{M}$ varies from $\dot{M}_c$ at the cold end (x=0 in figure 2–3) to $\dot{M}_h$ at the hot end (x=L). On the phasor diagram, $\dot{M}$ leads $\dot{M}_h$ by the angle ϕ and lags $\dot{M}_c$ by the angle θ–ϕ. In a physical sense then, ϕ represents position along the tube. Mass flow rate at any point in the tube is given below with the following boundary conditions:

$$m(x,t) = M(x)\cos(\omega t - \theta + \phi), \qquad (2\text{--}25)$$

where
$$\text{at } x=0, \quad \phi = \theta \text{ and } \dot{M} = \dot{M}_c, \qquad (2\text{--}26a)$$

24

and where $\qquad$ at x=L, $\quad \phi = 0$ and $\dot{M} = \dot{M}_h$. $\qquad$ (2–26b)

2.5   Dynamic Temperature Equation

Along with the mass flow rate, the dynamic temperature will be used to establish the enthalpy flow in the pulse tube. The development begins with the same energy balance on the pulse tube shown in eq (2–15). This equation is written for a point x along the tube and gives the result

$$\frac{d(\rho V_g u)}{dt} + \frac{d(\dot{m}h)}{dx} = 0. \qquad (2\text{–}27)$$

Using the continuity equation,

$$\frac{\partial \rho}{\partial t} + \frac{1}{A_g} \frac{\partial \dot{m}}{\partial x} = 0, \qquad (2\text{–}28)$$

and again the definitions of internal energy and enthalpy for an ideal gas (eqs (2–17) and (2–18)), we obtain the following differential equation:

$$\frac{\partial T}{\partial t} = \frac{RT}{C_p P} \frac{\partial P}{\partial t} - \frac{RT\dot{m}}{A_g P} \frac{\partial T}{\partial x}. \qquad (2\text{–}29)$$

If a small pressure ratio, $(P_d/P_a \ll 1)$ is assumed, $\Delta P/P$ and $\Delta T/T$ are small and the ratio T/P is equal to T_a/P_a. Equation (2–29) is then easily integrated over time to arrive at the phasor representation of the dynamic temperature in terms of the dynamic pressure ($\underline{P}_d$) and the total mass ($\underline{M}$) moved past point x in one–half cycle,

$$\underline{T}_d = \frac{RT}{C_p P_a} \underline{P}_d - \frac{RT_a}{A_g P_a} \frac{\partial T_a}{\partial x} \underline{M}. \tag{2-30}$$

The phasor diagram for $\underline{T}_d$ is shown in figure 2–5, where ψ is the phase angle between $\underline{T}_d$ and the total mass flow rate $\underline{\dot{M}}$. The first term of eq (2–30) is expressed in the time domain by substituting eq (2–23) for P_d. An expression for M in the time domain is found by integrating the total mass flow rate eq (2–25),

$$m(t) = (\dot{M}/\omega)\cos(\omega t - \theta + \phi - \pi/2) \tag{2-31}$$

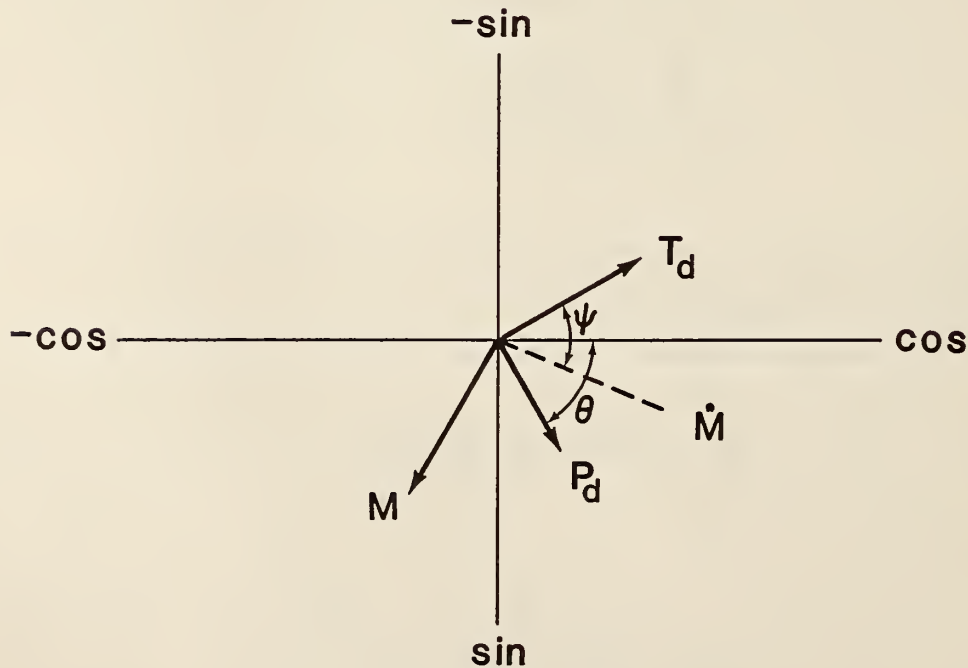
Figure 2–5. Phasor diagram for dynamic temperature and components.

The phase of $\underline{M}$ lags that of $\dot{M}$ by 90° and has a magnitude of $\dot{M}/\omega$. The time domain representation of the dynamic temperature is

$$T_d(x,t) = \frac{RT_a}{C_P}\left[\frac{P_d}{P_a}\right]\cos(\omega t - \theta) - \frac{RT_a}{A_g P_a}\frac{\dot{M}}{\omega}\left[\frac{\partial T_a}{\partial x}\right]\cos(\omega t - \theta + \phi - \pi/2). \tag{2-32}$$

2.6   Enthalpy Flow Equations (Models 1 and 2)

The average enthalpy flow is defined according to eq (2-12) as the integral of the product of $\dot{m}(x,t)$ and $T_d(x,t)$. Since the second term of T_d in eq (2-32) is 90o out of phase with respect to $\dot{m}$ in eq (2-25), the product of these terms, will integrate to 0 over one cycle. Therefore, the only contribution to $<\dot{H}>$ from the dynamic temperature is

$$\underline{T}_d = \frac{RT_a}{C_P P_a}\underline{P}_d\ . \tag{2-33}$$

Substituting eq (2-33) into eq (2-12) gives enthalpy flow in terms of dynamic pressure,

$$<\dot{H}> = \frac{RT_a}{\tau P_a^2}\int_0^\tau \dot{m}P_d\ dt. \tag{2-34}$$

Applying the time-domain expression for $\dot{m}$ and P_d results in an integral of the product of two cosines,

$$<\dot{H}> = \frac{RT_a}{\tau P_a^2}\dot{M}P_d\ \int_0^\tau [\cos(\omega t - \theta + \phi)\cos(\omega t - \theta]dt. \tag{2-35}$$

Performing the integration yields an expression for enthalpy flow in terms of the time-average temperature profile in the tube $T_a(x)$; the average pressure P_a ; amplitudes

of the mass flow rate and pressure $\dot{M}(x)$ and P_d ; and the phase angle between $\underline{\dot{M}}$ and $\underline{P_d}$, $\phi(x)$:

$$<\dot{H}> = \tfrac{1}{2} \frac{RT_a}{P_a} \dot{M}P_d \; \cos\phi. \qquad (2\text{--}36)$$

The phasor diagram in figure 2–4 provides a simple, geometric expression for ϕ,

$$\cos\phi = (\dot{M}_h/\dot{M})(T_h /T_a). \qquad (2\text{--}37)$$

$\dot{M}(x)$ and $T_a (x)$ cancel with the replacement of $\cos\phi$ in eq (2–36),

$$<\dot{H}> = \tfrac{1}{2} R\dot{M}_h T_h (P_d /P_a), \qquad (2\text{--}38)$$

and $<\dot{H}>$ does not depend on position x. Thus enthalpy flow becomes independent of position, and energy is conserved.

Equation (2–38) represents the net enthalpy flow or the gross refrigeration power in the OPTR. By rearranging this equation, several convenient dimensionless forms result. The first dimensionless equation is

$$\frac{<\dot{H}>}{<\dot{m}_c >RT_c} = \tfrac{\pi}{4}(P_d /P_a)(\dot{M}_h/\dot{M}_c)(T_h /T_c), \qquad (2\text{--}39)$$

where $<\dot{m}_c>$ is the mass flow rate at the cold end averaged over 1/2 cycle. Equation (2–39) shows that enthalpy flow per unit mass flow is proportional to the pressure ratio P_d /P_a , the mass flow ratio $\dot{M}_h/\dot{M}_c$, and the temperature ratio T_h /T_c . In terms of the phase angle θ, this equation is simply

28

$$\frac{<\dot{H}>}{<\dot{m}_c>RT_c} = \frac{\pi}{4}(P_d/P_a)\cos\theta. \tag{2-40}$$

The set of eqs (2–39) and (2–40) is called Model 1; this set is independent of dead volume in the system. These equations are useful for comparing performance per unit mass of the pulse tube to that of other cryocoolers.

For design purposes, an equation in terms of the swept volume of the compressor V_{cP} is desired. If dead volume in the system is neglected and if the compressor is assumed to be isothermal at ambient temperature T_h, the mass flow rate at the cold end is

$$\dot{M}_c = \dot{M}_{cP} = \frac{1}{2}M_{cP}\omega = \frac{1}{2}\frac{P_a V_{cP}}{RT_h}\omega, \tag{2-41}$$

and so

$$<\dot{m}_c> = \frac{2}{\pi}\dot{M}_c = 2\frac{P_a V_{cP} \nu}{RT_h} \tag{2-42}$$

since $\omega = 2\pi\nu$. M_{cP} represents the mass of fluid in the compressor and the maximum flow rate $\dot{M}_{cP}$ occurs when one–half of M_{cP} has left the compressor. Substituting for $<\dot{m}_c>$ in eq (2–39) results in the dimensionless form,

$$\frac{<\dot{H}>}{P_a V_{cp} \nu} = \frac{\pi}{2}(P_d/P_a)(\dot{M}_h/\dot{M}_c). \tag{2-43}$$

Equation (2–43) is useful for determining the cooling power available from a given compressor size. The refrigeration power for this case is proportional to the average pressure, the compressor volume, the frequency, the dynamic pressure ratio, and the mass flow ratio.

Another dimensionless enthalpy–flow equation can be developed for a pulse tube

with constant volume V_t. To do so, an expression relating the pressure ratio in the tube to the volume of the tube must be derived. The derivation begins with eq (2–20) from which the differential change in pressure due to mass flow at the tube ends can be derived. If the relationships in the time domain for the oscillating mass flow rates $\dot{m}_c$ and $\dot{m}_h$ are substituted in eq (2–20), integration over time t results in the following equation for pressure:

$$p(t) = \frac{\gamma R}{\omega V_t} [T_c \dot{M}_c \sin \omega t - T_h \dot{M}_h \sin(\omega t - \theta)]. \tag{2–44}$$

The integration is performed assuming T_c and T_h to be constant, which means the change in temperature for gas entering and leaving at the ends is small. The amplitude of the pressure oscillation is the dynamic pressure P_d , and using phasor algebra, the following equation is obtained:

$$P_d = \frac{\gamma R}{\omega V_t} [T_c^2 \dot{M}_c^2 + T_h^2 \dot{M}_h^2 - 2T_c T_h \dot{M}_c \dot{M}_h \cos \theta]^{\frac{1}{2}}. \tag{2–45}$$

After we factor out $\dot{M}_c$ and T_c, and we use eq (2–24) for $\cos \theta$, the dynamic pressure becomes

$$P_d \; = \frac{\gamma R T_c}{\omega V_t} \dot{M}_c \sin \theta. \tag{2–46}$$

Substituting for $\dot{M}_c$ using eq (2–41) gives the pressure ratio in terms of the compressor volume and the pulse tube volume,

$$P_d / P_a \; = \frac{\gamma}{2} (V_{cp} / V_t) (T_c / T_h) \sin \theta. \tag{2–47}$$

The above equation is appropriate for a reversible, adiabatic process with zero dead volume between the compressor and the tube.

After we use eqs (2–43) and (2–47), two dimensionless equations for enthalpy flow for a given pulse tube volume can be written in terms of the dynamic pressure ratio and the volume ratio:

$$\frac{<\dot{H}>}{P_a \, V_t \, \nu} = \frac{\pi}{\gamma} \left(P_d / P_a\right)^2 (\dot{M}_h / \dot{M}_c)(T_h / T_c)[1 - (\dot{M}_h / \dot{M}_c)^2 (T_h / T_c)^2]^{-1/2}, \qquad (2\text{–}48)$$

and

$$\frac{<\dot{H}>}{P_a \, V_t \, \nu} = \frac{\pi}{4} \left(V_{CP} / V_t\right)^2 (\dot{M}_h / \dot{M}_c) \, (T_c / T_h)[1 - (\dot{M}_h / \dot{M}_c)^2 (T_h / T_c)^2]^{-1/2}. \qquad (2\text{–}49)$$

The equations can be simplified by writing them in terms of θ,

$$\frac{<\dot{H}>}{P_a \, V_t \, \nu} = \frac{\pi}{\gamma} \left(P_d / P_a\right)^2 \cos\theta, \qquad (2\text{–}50)$$

and

$$\frac{<\dot{H}>}{P_a \, V_t \, \nu} = \gamma \frac{\pi}{4} \left(V_{CP} / V_t\right)^2 (T_c / T_h)^2 \sin\theta \, \cos\theta. \qquad (2\text{–}51)$$

Equation (2–50) shows that the dimensionless enthalpy flow increases with the square of the dynamic pressure ratio. If this ratio is constant, the enthalpy flow decreases as the heat capacity ratio γ of the working fluid increases. According to eq (2–51), enthalpy flow increases with the square of the volume ratio and, if this ratio is constant, increases as γ increases. The set of eqs (2–43), (2–50), and (2–51) is called Model 2.

2.7   Dead Volume in Pulse Tube Systems (Model 3)

Dead volume in pulse tube systems is very important for design. Up to this point, the model of refrigeration power has ignored extra volume between the compressor and the pulse tube. In real systems, this volume exists in connective tubing and in the regenerator and will significantly affect performance. In the ideal system with no dead volume, $\dot{m}_c =$ $\dot{m}_{cp}$. In the real system, mass must be used to pressurize the extra volume, which means mass flow at the cold end will be less than the flow rate at the compressor. The smaller mass flow results in a lower pressure ratio and a loss of cooling power.

A new equation for mass flow at the cold end will now be derived for a mass balance on the dead volume between the compressor and the pulse tube. The system is shown in figure 2–6, and the mass balance is

$$dM_D/dt = \underline{\dot{M}}_{cP} - \underline{\dot{M}}_c. \tag{2–52}$$

The phasors in eq (2–52) are displayed on the phasor diagram for the mass flow rate in figure 2–4. M_D is the mass of fluid in the dead volume which is assumed to be isothermal at temperature T_h . Therefore,

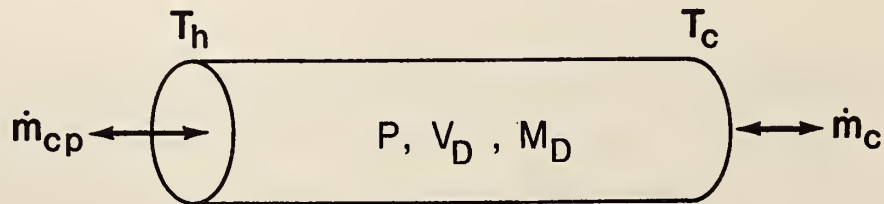$$\frac{V_D}{RT_h} \frac{dP}{dt} = \underline{\dot{M}}_{cP} - \underline{\dot{M}}_c. \tag{2–53}$$

Figure 2–6. Isothermal dead volume system between compressor and pulse tube.

In terms of phasors, dead volume creates a phase shift, so $\underline{\dot{M}}_c$ lags $\underline{\dot{M}}_{cP}$ by the phase angle α. The mass balance can be written in the time domain as

$$\frac{V_D}{R T_h} \frac{dp}{dt} = \dot{M}_{cP}\cos(\omega t + \alpha) - \dot{M}_c\cos\omega t.$$ (2–54)

Integrating eq (2–54) results in an equation for pressure,

$$p(t) = \frac{R T_h}{\omega V_D} [\dot{M}_{cP}\sin(\omega t + \alpha) - \dot{M}_c\sin\omega t].$$ (2–55)

Again, phasor algebra provides an expression for pressure amplitude:

$$P_d = \frac{R T_h}{\omega V_D} [\dot{M}_{cP}^2 + \dot{M}_c^2 - 2\dot{M}_{cP}\dot{M}_c\cos\alpha]^{\frac{1}{2}}.$$ (2–56)

We make use of figure 2–4, and applying a trigonometric identity and the law of sines, $\cos\alpha$ is written in terms of θ,

$$\cos\alpha = (\dot{M}_c + \frac{dM_D}{dt}\sin\theta)/\dot{M}_{cP},$$ (2–57)

where the amplitude of the change in mass in the dead volume is

$$\frac{dM_D}{dt} = \frac{P_d V_D}{R T_h}\,\omega.$$ (2–58)

Substituting eq (2–57) into (2–56) results in an equation containing the dynamic pressure amplitude P_d and the mass flow rate amplitude $\dot{M}_c$,

$$\left(\frac{P_d\, V_D}{R\, T_h}\, \omega\right)^2 \dot{M}_{cP}^2 + \dot{M}_c^2 - 2\dot{M}_c \left(\frac{P_d\, V_D}{R\, T_h}\, \omega\right)\sin\theta. \tag{2-59}$$

Equation (2–59), along with an expression containing P_d derived from a mass balance on the pulse tube volume shown in eq (2–53), are then solved simultaneously to produce expressions for P_d / P_a and $\dot{M}_c$:

$$P_d / P_a = \frac{1}{2}\, (V_{cP}/V_D)\, \sin\theta(V^*)^{\frac{1}{2}}, \tag{2-60}$$

and

$$\dot{M}_c = \frac{1}{\gamma}\, \dot{M}_{cP}\, (V_t/V_b)\, (T_h/T_c)/(V^*)^{\frac{1}{2}}, \tag{2-61}$$

where

$$V^* = [(1/\gamma^2)(V_t/V_b)^2(T_h/T_c)^2 + \{(2/\gamma)(V_t/V_b)(T_h/T_c)+1\}\sin 2\theta]. \tag{2-62}$$

V^* is considered to be an effective volume ratio for an OPTR System with dead volume, mass flow through the orifice, and an adiabatic tube.

After we substitute eqs (2–60) and (2–61) into eq (2–39) (using the definition $<\dot{m}_c> = \frac{2}{\pi}\, \dot{M}_c$), the dimensionless enthalpy flow for pulse tube systems with dead volume is

$$\frac{<\dot{H}>}{P_a\, V_t\, \nu} = \frac{1}{\gamma}\frac{\pi}{2}\, (P_d / P_a)(V_t / V_b)\, \cos\theta/V^*, \tag{2-63}$$

or

$$\frac{\langle \dot{H} \rangle}{P_a\, V_t\, \nu} = \frac{1}{\gamma} \frac{\pi}{4} (V_{cp}/V_D)(V_t/V_D)\ \cos\theta \sin\theta / V^*. \qquad (2\text{--}64)$$

Equations (2--63) and (2--64) are in the same form as that of eq (2--50) and (2--51) and show enthalpy flow in terms of the pressure ratio P_d/P_a and the volume ratio V_{cp}/V_D respectively. They represent Model 3.

CHAPTER 3
EXPERIMENTAL INVESTIGATION

3.1 Test Apparatus

The experimental pulse tube apparatus was designed to provide both convenient and accurate measurements of important parameters for the calculation of refrigeration power and mass flow rate. A schematic of the apparatus is shown in figure 3--1. The regenerator, pulse tube, and two units called isothermalizers are contained within the cryostat, while the orifice and reservoir are located outside at room temperature. A vacuum of 10^{-2} P_a (10^{-4} Torr) or lower is maintained in the cryostat, and the components within are surrounded by a copper radiation shield maintained at 77 K by an LN_2 bath. The hot--end heat exchanger of the pulse tube, where measurements of gross refrigeration are made, is carefully insulated from the radiation shield with several layers of aluminized Mylar.

All experimental measurements were carried out using a stainless steel pulse tube of length 130 mm and diameter of 19.1 mm ($V_t = 31.9$ cm^3). The isothermal ends of the pulse tube consist of two copper caps filled with 80--mesh copper screen to ensure good heat transfer between the gas and the cooling water. The screen also helps to align the flow in the tube and decreases turbulence which degrades the temperature gradient. The volume of each of the hot--and cold--end heat exchangers is about 10% of the pulse tube volume. Conductive losses along the stainless steel pulse tube were calculated to be less than 1% of the refrigeration capacity.

The regenerator was constructed of a stainless steel tube 19 mm in diameter by 127 mm long packed with 1050 discs of 150--mesh, phosphor--bronze screen. The void volume in this regenerator was 21.6 cm^3 and dead volume in the system between the compressor

and the pulse tube was 50 cm³. The hot end of the regenerator had a water—cooled heat exchanger made up of 80—mesh copper screens. This heat exchanger ensures that gas entering the regenerator is at ambient temperature. The orifice consists of a 15—turn needle valve and the volume of the reservoir located above the orifice is approximately 1000 cm³.

In previous work by Radebaugh, two isothermalizer units were inserted between the regenerator and the pulse tube in order to isolate regenerator loss from intrinsic refrigeration. The isothermalizers have a large thermal mass with high heat capacity to prevent temperature oscillations. There is excellent heat transfer with the working fluid which flows through two small, annular gaps 178 μm thick. In past experiments, the two isothermalizers were maintained at the same temperature by cooling the first with N_2 boil—off and heating isothermalizer 2 with an electrical heater. Heat removed from isothermalizer 1 represents the regenerator loss, and heat supplied to isothermalizer 2 represents the net refrigeration power. In this work, isothermalizer 1 was not cooled since only measurements of gross refrigeration at the hot end of the pulse tube were needed.

The reciprocating compressor was valveless and nonlubricated with a total swept volume of 290 cm³. The variable—frequency drive used was capable of providing frequencies up to 12 Hz.

3.2   Measurements and Calculations

Figure 3—1 indicates points in the apparatus where temperature and pressure were measured. A variable reluctance pressure transducer was located at the hot end of the pulse tube, near ambient temperature, to measure the absolute pressure oscillation. A similar pressure transducer is used in the isothermalizer 2, where flow is laminar and essentially isothermal, to measure pressure drop for calculation of the mass flow rate in the pulse tube. Since the isothermalizer is at the cold end temperature, the temperature dependence of the transducer sensitivity was determined in a previous experiment [23]. The sensitivity was found to vary by less than 13% between 300 K and 77 K so this variation was ignored. However, the zero setting of the pressure transducer changed significantly with temperature and was therefore reset for each new measurement. A third pressure transducer of the piezoresistive type was used to measure the absolute pressure oscillation in the reservoir volume. The uncertainty in each of the readings of the three pressure transducers was ±1 mV (±1 kPa).
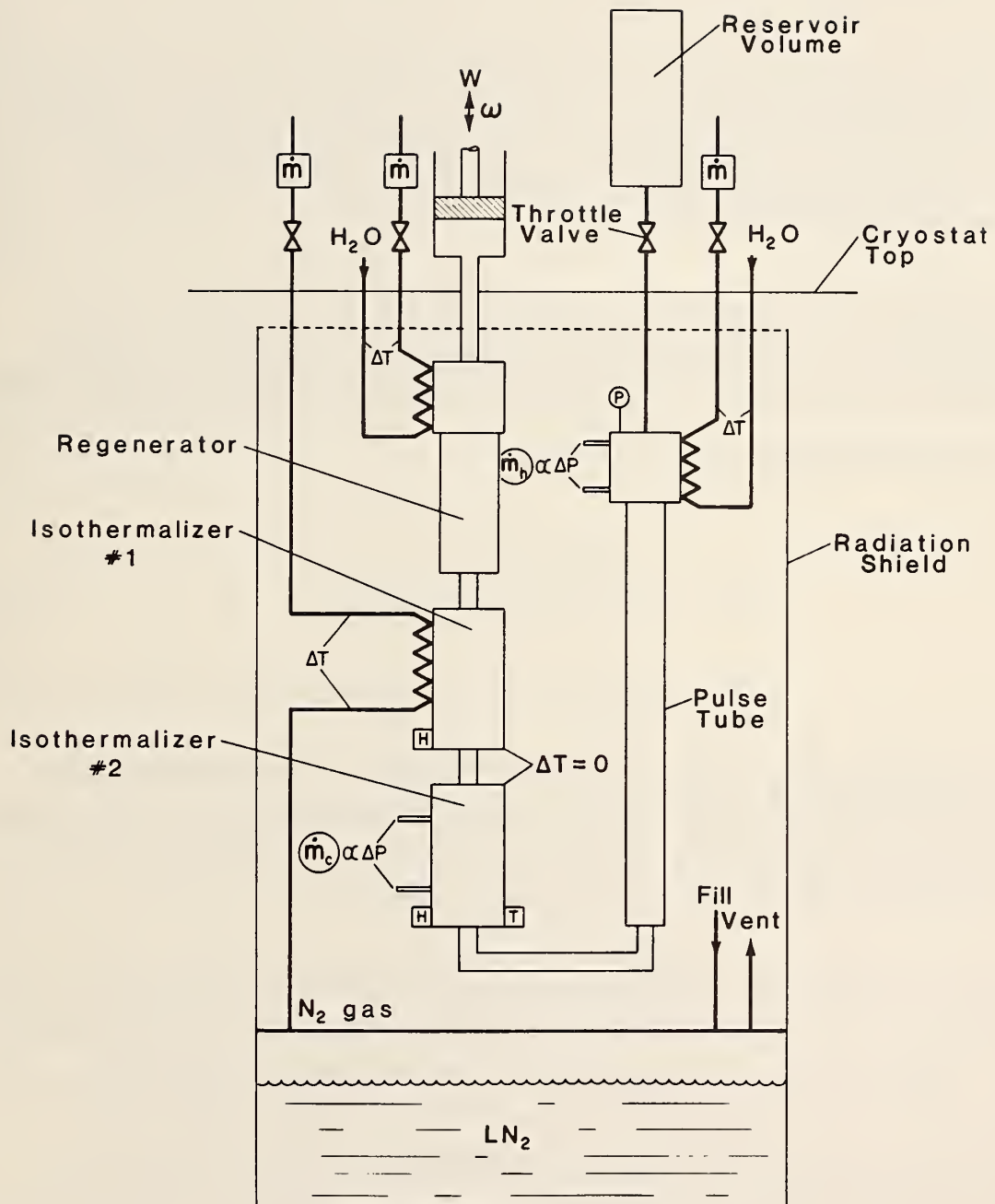
Figure 3–1. Schematic of test apparatus.

The three pressure oscillations, along with the temperature oscillation in the pulse tube (see temperature experiment), were collected on a processing digital oscilloscope. The oscilloscope is capable of reading voltage with 12–bit resolution and an accuracy of ±0.75 percent.

Absolute temperatures at the cold and hot ends of the pulse tube were measured with diode thermometers accurate to ±1 K. The difference in temperature between the water inlet and outlet in the hot end heat exchanger was measured with a type–T (copper/Constantan) thermocouple.

An equation for the mass flow rate $<\dot{m}_c>$ at the cold end of the pulse tube was developed to account for density and viscosity variations with temperature. Measured values of the pressure drop ΔP and the pressure ratio P_h/P_ℓ across the laminar flow element in the isothermalizer are used as follows:

$$<\dot{m}_c> = \left[\frac{\rho_2}{2}\right]\left[\frac{P_h}{P_\ell} + 1\right]\frac{\Delta P}{\mu_c Z_f}, \qquad (3–1)$$

where ρ_a is the density of the gas at the average pressure and at T_c, μ_c is the viscosity at T_c, and Z_f is the flow impedance for the annular gaps in the isothermalizer. The factor Z_f was determined experimentally from ΔP data at different flow rates. Equation (3–1) is valid for laminar flow, and the derivation is shown in Appendix A.

Flow of both He and N_2 through the isothermalizer remains laminar for mass flow rates up to about 2.5 g/s. For helium, flow rates were never greater than 2 g/s; however, the flow rates with nitrogen were much higher and turbulent flow was encountered. Therefore, eq (3–1) could not be used for N_2, and a trial–and–error procedure was necessary to solve for the mass flow rate. This procedure is presented in Appendix A.

The mass flow rate through the orifice can be expressed simply as the amount of mass moved in one direction divided by one half the period. For an ideal gas, adiabatic flow, and a small pressure oscillation in the reservoir, the average flow rate is proportional to the change in pressure in the reservoir as follows:

$$<\dot{m}_h> = \frac{\Delta m_h}{\tau / 2} = \frac{2\Delta P_r V_r}{\gamma R T_r \tau}, \tag{3--2}$$

where V_r and T_r are the volume and temperature of the reservoir, ΔP_r is the difference between the maximum and minimum pressures in the reservoir, R is the gas constant, and τ is the period. Because a significant amount of gas is moving through the orifice at a high velocity, adiabatic flow is a good assumption. Also, the pressure variation in the reservoir was very small ($\Delta P_r / P_r < 0.02$), so eq (3--2) is valid for this pulse tube system. The derivation is shown in Appendix A.

Gross refrigeration was found by measuring the flow rate $\dot{m}$ and the temperature change ΔT of the water flowing through the cooling coil at the hot end of the tube according to the equation

$$\dot{Q} = \dot{m}C_p\Delta T, \tag{3--3}$$

The measurements of gross refrigeration were accurate to $\pm 7\%$.

In order to calculate the efficiency of the pulse tube, it is necessary to find the work input rate $\dot{W}$. Because the compressor used to drive the pulse tube was not designed specifically for this work, it is oversized and inefficient. Therefore, the electrical power input to the compressor motor is not a good measurement of the work input required by the pulse tube. However, by calculating the ideal thermodynamic work input from pressure measurements, losses associated with the regenerator and the compressor are bypassed and only the efficiency of the cooling process is measured. This is the best method for comparing the efficiency of the OPTR to that of other refrigerators.

The input rate of ideal thermodynamic work is determined from the measurements of the mass flow rate oscillation at the cold end $\dot{m}_c(t)$ and the absolute pressure oscillation in the pulse tube $p(t)$. For a closed cycle the work input is

$$W = pdV, \tag{3--4}$$

where V is the volume of the gas in the compressor, and is derived from the gas density and $m_c(t)$. The work input over one cycle is

$$W = \int_0^T p(t) \frac{dV(t)}{dt} dt. \qquad (3\text{--}5)$$

The average rate of work input is found by dividing by the period,

$$<W> = \frac{1}{\tau} \int_0^T p(t) \frac{dV(t)}{dt} dt. \qquad (3\text{--}6)$$

The coefficient of performance

$$(COP)_{Pt} = <\dot{Q}>/<W>, \qquad (3\text{--}7)$$

of the pulse tube can then be calculated using time–averaged values of $\dot{Q}$ and $\dot{W}$, and compared to the COP for a Carnot cycle to determine the thermodynamic efficiency relative to Carnot efficiency:

$$\eta = (COP)_{Pt}/(COP)_c = [<\dot{Q}>/<W>][T_c/(T_h\text{--}T_c)]. \qquad (3\text{--}8)$$

Here, η is the thermodynamic efficiency only for the cooling process in the pulse tube and is useful for comparison with other refrigeration cycles.

All calculations for $\dot{m}_h(t)$, $\dot{m}_c(t)$, $V(t)$, and $\dot{W}$ were performed on the processing digital oscilloscope.

3.3   Effect of Pressure on Performance

The analytical model indicates that the average pressure and the ratio of dynamic pressure to average pressure are two important parameters in describing enthalpy flow in the orifice pulse tube. These pressure parameters have not previously been studied experimentally. The objective of this experiment is to verify the dependency of refrigeration power on P_a and P_d/P_a as predicted by the model. Equation (2–50) shows that refrigeration power is a linear function of P_a and a quadratic function of P_d/P_a. This equation is particularly convenient since dimensionless enthalpy flow is in terms of pulse tube volume and not compressor volume. The working volume of the compressor in the experimental apparatus was varied in order to obtain data at different pressure ratios.

Refrigeration capacity was measured on the same OPTR as described earlier. The frequency and the cold end temperature were kept constant at 6 Hz and 200 K, and the orifice valve was set at three turns unless otherwise noted. The first set of measurements was made at average pressures of 0.5, 1.0, and 1.5 MPa, with $\dot{m}_h/\dot{m}_c = 0.28$ and $P_d/P_a = 0.29$. Care was taken to assure that the compression ratio in these measurements was constant because, as will be shown, the refrigeration capacity changes rapidly with P_d/P_a.

In the second set of measurements, the average pressure was kept constant at 1.0 MPa. The pressure ratio P_d/P_a was varied from 0.9 to 0.39 with $\dot{m}_h/\dot{m}_c = 0.26$. Different compression ratios were achieved by adjusting a bypass valve between the inlet to the refrigerator and ballast volume.

The results of this set of experiments are compared to the analytical model represented by eq (2–50). This dimensionless equation is expressed in terms of the pulse tube volume, which is constant throughout this work. The model shows that refrigeration power is proportional to the average pressure. The experimental results are shown in figure 3–2. Even though tests were conducted at only three different pressures, the data points fall very close to the best–fit line, with a coefficient of correlation $r^2 = 0.99$. The plot clearly demonstrates the linear dependence of refrigeration power on the average pressure, as predicted by the analytical model.

The results of experimentally varying the pressure ratio compare equally well with the theoretical model. Equation (2–50) shows that the refrigeration power increases with the square of P_d/P_a and figure 3–3 confirms this result. For this plot, $r^2 = 0.99$ and the

41

best–fit curve shown by the solid line has an exponent of 2.10.

3.4   Effect of Working Fluid on Performance

The second experiment was designed to determine the effect of a different working fluid on performance of the OPTR. Up to this point, helium has been used in all experiments. Nitrogen was chosen as the second working fluid, and refrigeration power was measured for comparison with the helium data. Recall that eq (2–51) of the analytical model shows that dimensionless enthalpy flow increases with γ, the ratio of heat capacities, for a constant ratio of compressor volume to pulse tube volume (V_{cp}/V_t). Equation (2–50) shows that enthalpy flow increases with $1/\gamma$ for a constant ratio of dynamic pressure to average pressure (P_d/P_a). In order to test eq (2–51), measurements with nitrogen were taken at the same volume variation of the compressor (bypass valve completely closed) as previously used with helium. The pressure ratios for this case were $P_d/P_a = 0.39$ for helium and $P_d/P_a = 0.27$ for nitrogen. Then, to test eq (2–50), the compressor volume variation was decreased (bypass valve partially open) and refrigeration measurements were made with helium at the same pressure ratio as nitrogen. The average pressure was kept at 1.0 MPa with $\nu = 6$ Hz and $T_c = 200$ K as before.
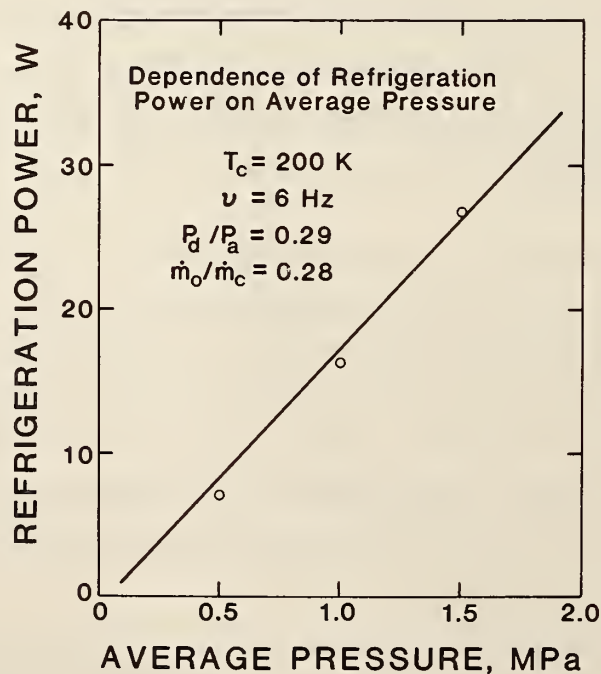
Figure 3–2.   Experimental measurements of refrigeration power as a function of the average tube pressure.
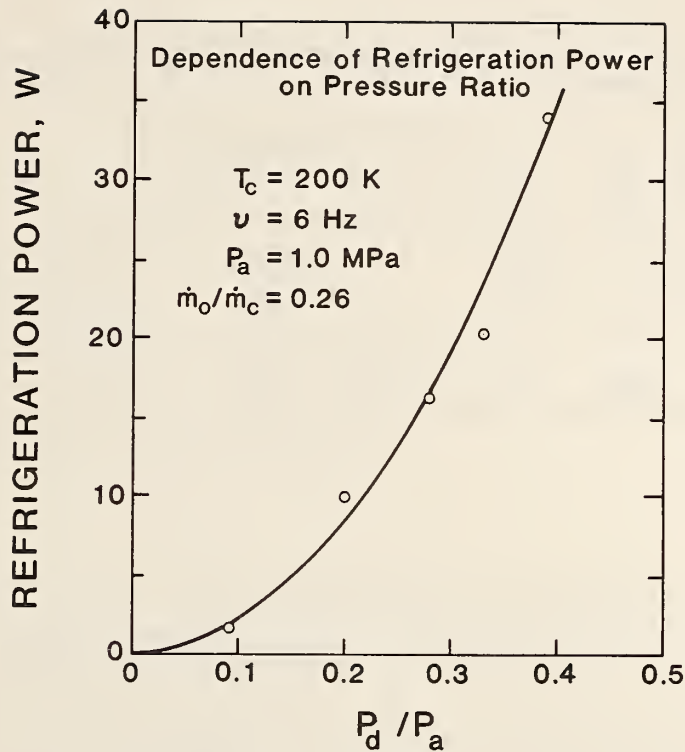
Figure 3–3.   Experimental measurement of refrigeration power as a
                   function of the ratio of dynamic pressure to average pressure.

A typical sample of the data used for comparison of the two working fluids
(including the refrigeration power and important system parameters) is presented in table
3–1. Care was taken to keep the system parameters as nearly constant as possible for each
case. For instance, with nitrogen it was necessary to open the orifice valve to 10 turns in
order to match the mass flow ratio attained with helium at three turns of the valves. The
first set of helium data in table 3–1 ($\dot{Q} = 18.1$ W) is for the case of constant P_d/P_a and the
second set of data ($\dot{Q} = 29.9$ W) is for the case of constant V_{cp}/V_t.

Table 3–1. Experimental refrigeration power and system
parameters for N_2 and He

	$\dot{Q}$ (W)	T_c (K)	P_a (kPa)	ν (Hz)	P_d/P_a	$\dot{m}_h/\dot{m}_c$	γ
N_2	14.8	200.0	1059	6.08	0.28	0.18	1.40
He	18.1	200.0	1052	6.10	0.29	0.24	1.67
He	29.9	200.0	1069	6.07	0.29	0.20	1.67

The experimental and analytical results are displayed in table 3–2 as ratios of refrigeration power for convenient comparison. The first column in table 3–2 shows that about 1.2 times more refrigeration capacity was measured for helium than for nitrogen with constant P_d/P_a. Also, about twice the capacity was measured for helium with a constant V_{cp}/V_t. The third column of Table 3–2 shows the ratios predicted by the model. For constant volume ratio, eq (2–51) says $\dot{Q}_{He}/\dot{Q}_{N_2} = \gamma_{He}/\gamma_{N_2} = 1.103$; while for a constant pressure ratio, eq (2–50) says $\dot{Q}_{He}\,\dot{Q}_{N_2} = \gamma_{N_2}/\gamma_{He} = 0.838$ when other system parameters are held constant. Although values of P_a, ν, P_d/P_a, and $\dot{m}_h/\dot{m}_c$ for the different cases are nearly equal, the differences are large enough to affect the refrigeration ratios. Therefore the experimental ratios were corrected for these differences and are shown in the second column of Table 3–2. Calculations for values in Table 3–2 are given in Appendix A.

The corrected refrigeration ratio for constant P_d/P_a, 0.848, nearly matches the ratio predicted by the model, 0.838. This indicates that eq (2–50) gives a valid description of the dependence of refrigeration power on the working fluid. Since $\dot{Q}_{He}/\dot{Q}_{N_2} = \gamma_{N_2}/\gamma_{He}$, nitrogen produces a slightly larger refrigeration capacity than helium for the same pressure ratio.

On the other hand, the corrected refrigeration ratio for a constant V_{cp}/V_t, 1.856, is much larger than the ratio $\gamma_{He}/\gamma_{N_2} = 1.193$ as predicted by the model. However, we suspected that, even though the same setting of compressor volume was used for both nitrogen and helium, the effective volume ratio may not have been the same. A short

Table 3.2. Comparison of refrigeration ratios

	$(\dot{Q}_{He}/\dot{Q}_{N_2})EXP$	$(\dot{Q}_{He}/\dot{Q}_{N_2})EXP_c$	$(\dot{Q}_{He}/\dot{Q}_{N_2})$ Model
constant (P_d/P_a)	1.226	1.848[1]	0.838
constant (V_{cP}/V_t)	2.026	1.856[1]	1.103

[1]These experimental values are corrected for slight differences between the He and N_2 runs in P_a, ν, P_d/P_a, and $\dot{m}_h/\dot{m}_c$

experiment was devised to test this idea.

The test consisted of measuring the pressure ratio in the pulse tube and at the outlet of the compressor for both helium and nitrogen with the apparatus running at room temperature. Because of the volume of the regenerator, two isothermalizers, and a significant amount of volume in the connective tubing between the compressor and the pulse tube, a significant pressure drop exists for flow between these two components. Therefore we anticipate that the pressure ratio in the pulse tube would be less than that in the compressor. The measurements shown in table 3–3 confirm this idea, and they also show that the pressure drop was significantly greater for nitrogen than for helium.

The larger pressure drop associated with nitrogen is attributed to the fact that the flow for nitrogen in the regenerator and isothermalizers was turbulent. Since nitrogen has a much larger density and a slightly lower viscosity than helium, the mass flow rates for nitrogen were about five times greater than those for helium (see eq (3–1)). While flow for helium was clearly laminar with a Reynolds number of about 800, flow for nitrogen became turbulent with a Reynolds number of about 10 000. The large flow rate of nitrogen then translates into a large pressure drop, as shown by the following equation:

$$\Delta P = \frac{\dot{m} R_e \mu L}{8 \rho A_g r_h^2}. \qquad (3–9)$$

45

Table 3–3. Pressure ratios

	(P_d/P_a) Compressor	(P_d/P_a) Pulse Tube
He	0.50	0.42
N2	0.54	0.35

The problem with a large pressure drop is that less gas volume is moved through the pulse tube which in turn decreases the amount of refrigeration produced. The considerable difference in volume of nitrogen moved compared to that of helium explains the high experimental value for $\dot{Q}He/\dot{Q}N_2$ in table 3–2. Therefore it is not possible to directly verify the dependence of refrigeration power on γ for constant V_{cp}/V_t with the present test apparatus. However, since eq (2–50) and (2–51) are essentially different forms of the same eq and (2–50) was verified, we think that (2–51) is also valid.

3.5 Effect of Frequency and Mass Flow Ratio on Performance

Pulse frequency and mass flow ratio are two more parameters that needed to be studied to further verify the analytical model. However, experimental work was not necessary in this case since useful data were available from experiments previously performed by Herrmann and Radebaugh in 1986 [23], [24]. These experiments were carried out on the same apparatus as used in this study and under the same working conditions. Three different pulse tubes were studied for which refrigeration power was measured at different frequencies and different orifice settings for cold–end temperatures down to 80 K. The data used for comparison with the model were taken for a pulse tube with different dimensions but with the same volume as the tube tested here.

Refrigeration power as a function of frequency is plotted in figure 3–4. The data were carefully chosen to be sure that only the frequency was varying and that other parameters, P_a, P_d/P_a, T_c, and $\dot{m}_h/\dot{m}_c$, important to the refrigeration power were kept constant. According to the model, the refrigeration power increases linearly with the frequency. This is exactly the result seen in figure 3–4, in which three of the measured
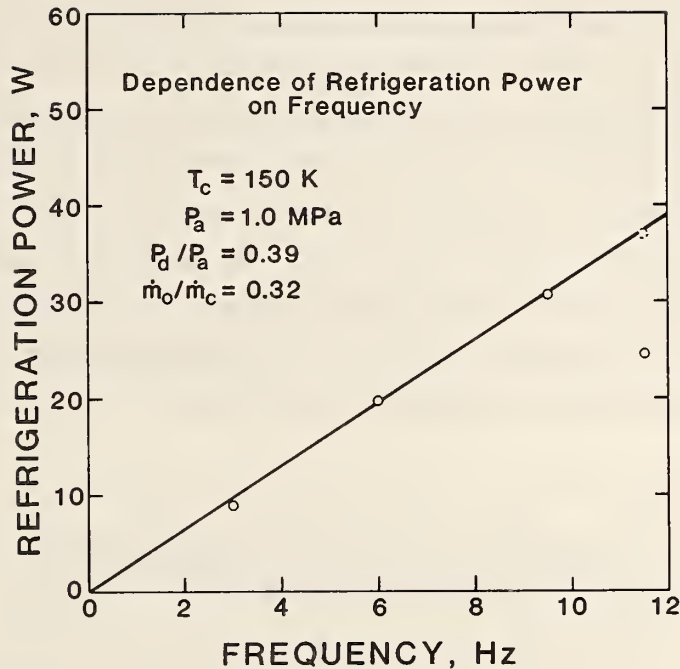
Figure 3–4.   Measurements of refrigeration power as a
                   function of pulse frequency.

data points fit the best–fit line with $r^2 = 0.99$. The fourth point at 11.5 Hz deviated greatly from the linear behavior; however this measurement was taken at a different P_d/P_a and, once corrected, also conformed to the same linear dependence.

The fact that the refrigeration power exhibits a linear dependence on the frequency indicates that the average enthalpy flow in the tube is constant over one cycle. For $T_c = 150$ K, $P_a = 1$ MPa, $P_d/P_a = 0.39$, and $\dot{m}_h/\dot{m}_c = 0.32$, an enthalpy flow of approximately 3 J/cycle was observed. The more cycles that can be completed in a time period the greater the enthalpy flow rate. Theoretically then there is no optimum frequency. Of course in practice this is not true since pressure drop and ineffectiveness in the regenerator degrade performance at the higher frequencies. There is also a limit imposed by the flow impedance of the orifice valve in which further increase in the frequency decreases flow through the orifice.

A second parameter that was studied using data from previous experiments is the

mass flow ratio $\dot{m}_h/\dot{m}_c$. Measurements were taken with the orifice valve open to 1/2, 1, 2, and 3 turns giving a range of flow ratios from 0.2 to 0.75 at $\nu = 6$ Hz and $P_d/P_a = 0.4$. The model says that $\dot{Q}$ has a linear dependence on $\dot{m}_h/\dot{m}_c$. The plot of experimental data in figure 3–5 for $T_c = 188$ K, $\nu = 6$ Hz, $P_a = 1$ MPa, and $P_d/P_a = 0.40$ confirms this behavior. The data provide an excellent linear fit with a coefficient of correlation of $r^2 = 1.00$. It is puzzling that the plot seems to show that for $\dot{m}_h/\dot{m}_c = 0$ (orifice closed), the refrigeration power will be zero. Although small compared to refrigeration power with the orifice open, cooling has certainly been observed with the orifice closed; this is due to small but nonzero heat transfer between the gas and the tube wall.
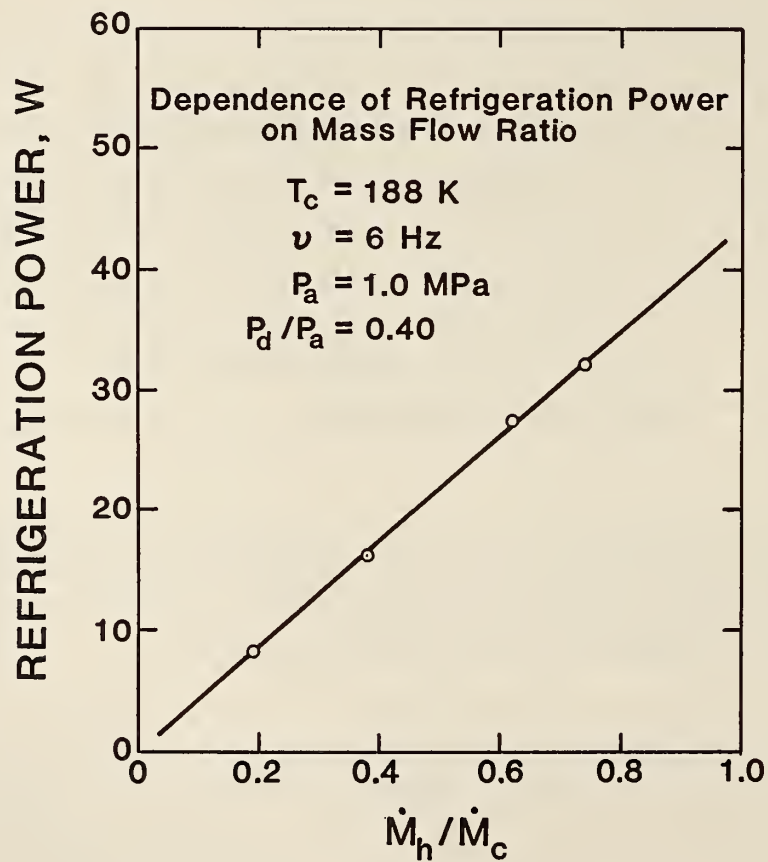

Figure 3–5.   Measurements of refrigeration power as a function of the ratio of mass flow through the orifice to mass flow due to the compressor.

3.6   Measurement of Gas Temperature Profile in the Pulse Tube

The temperature oscillation is important for understanding the cooling mechanism in the OPTR. From the development of the model, the time–averaged gas temperature T_a and the phase angle ψ between the temperature oscillation and the mass flow rate oscillation are important parameters in determining the enthalpy flow. Measurements of the gas temperature profile in the tube would allow for the calculation of the actual enthalpy flow as a function of position in the tube. Temperature measurements would also provide useful information on the behavior of the dynamic temperature T_d and phase shift ψ along the tube.

A probe was devised to sample gas temperatures at different points along the tube. The probe consists of a type E, Chromel/Constantan (nickel–chromium/copper–nickel) thermocouple attached to one end of a 3 mm diameter stainless steel tube. Since an accurate measurement of the amplitude of the dynamic temperature is desired, a foil type thermocouple, 0.0127 mm thick, was chosen to provide a fast response. The response time was calculated to be 8 ms, which is an order of magnitude less than the heat transfer period available during operation at 6 Hz. The thermocouple tip extends 1 cm from the end of the tube, which was sealed with epoxy. The temperature probe was inserted into the pulse tube through an O–ring seal at the top of the cryostat as shown in figure 3–6. The gas temperature could be sampled at any position along the tube during operation and measurements were generally made at 1 cm intervals.

Four temperature profiles were measured with the orifice opened to three turns for cold–end temperatures of 275, 200, 150, and 110 K. One profile was measured with the orifice closed at 200 K. Each measurement consisted of approximately six cycles of the temperature oscillation which were collected and stored on the digital oscilloscope. Care was taken to make sure the system was at equilibrium when the data were collected and also that T_c was the same for each measurement along the tube. The temperature profiles are for helium at an average pressure of 1.0 MPa and a frequency of 6 Hz.
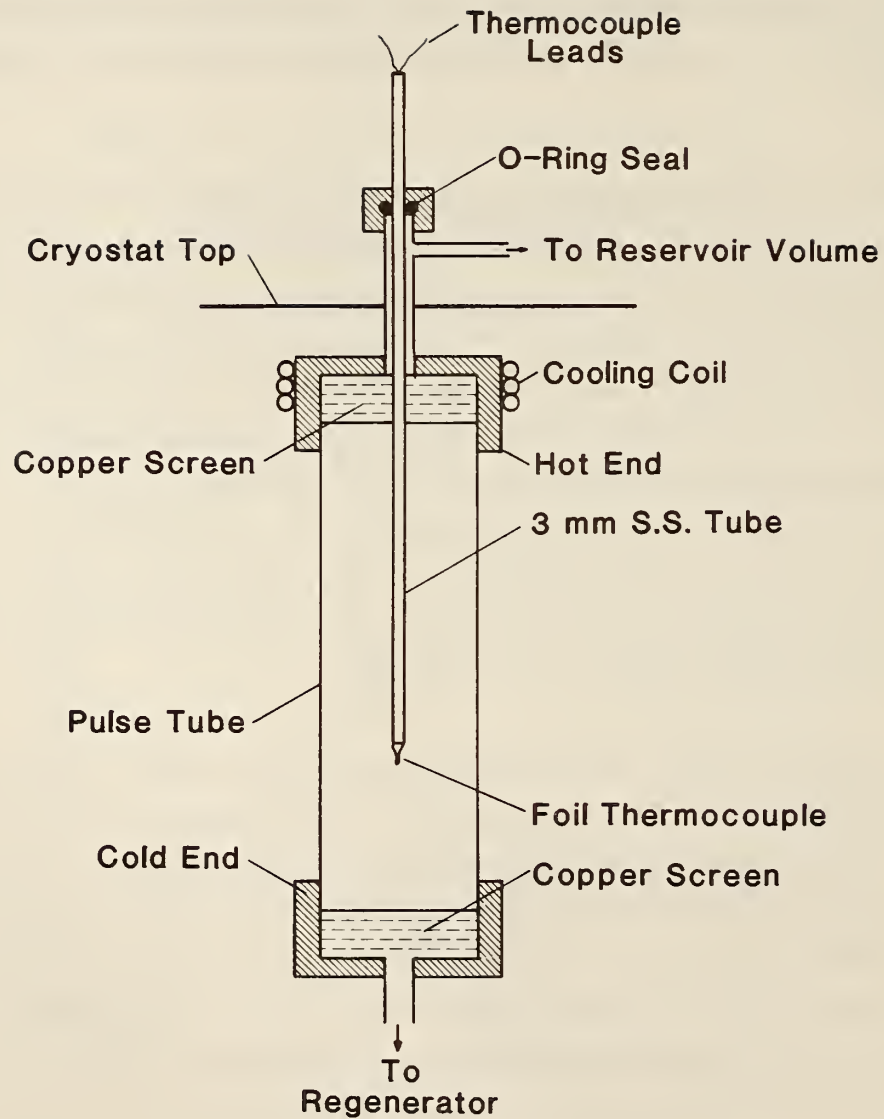
.

Figure 3–6.   Temperature probe with foil Chromel/
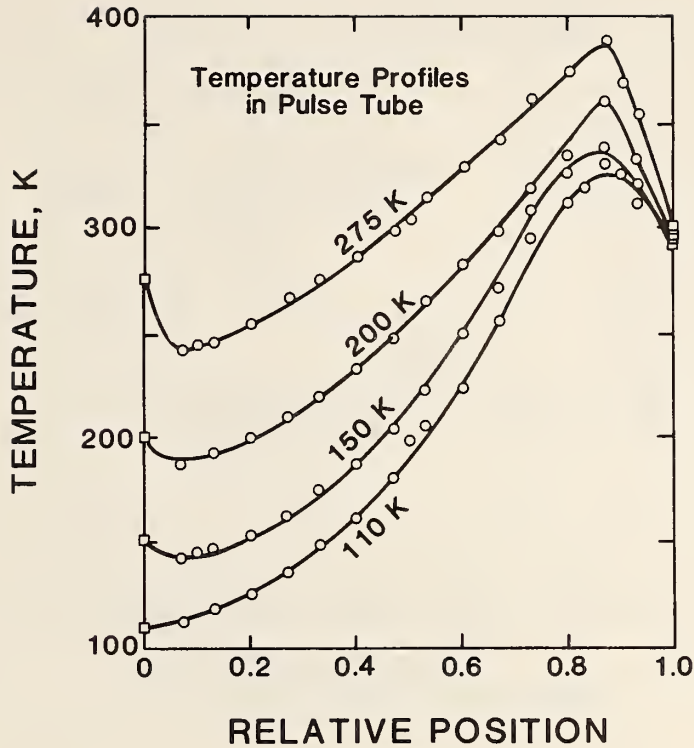Constantan thermocouple.

Figure 3–7.   Average gas temperature as a function of position
in the tube for different cold end temperatures with the
orifice open.

The first set of results obtained from these measurements is the time–averaged temperature profiles. Figure 3–7 shows average temperature vs relative position in the tube for the four cold–end temperatures with the orifice open. The circles represent measurements taken with the thermocouple probe, while the squares represent temperatures measured with the diode thermometers on the isothermal heat exchangers at the ends of the tube. The average gas temperature changes linearly over the middle 60% of the tube. We anticipate that the true gas temperature at the hot end would be slightly above the hot–end temperature measured by the diode due to the finite ΔT needed for heat transfer. For the same reason, the gas at the measured cold end should be slightly cooler than the cold–end temperature. However, the slopes of these profiles are great enough to put the points just before the two ends well above the hot end temperature and well below the cold end temperature. In contrast, figure 3–8 shows that the temperature profile with the orifice closed is much flatter than that with the orifice open. For $T_c = 200$ K, the slope of the profile with the orifice open is twice as large as the slope with the orifice closed. In
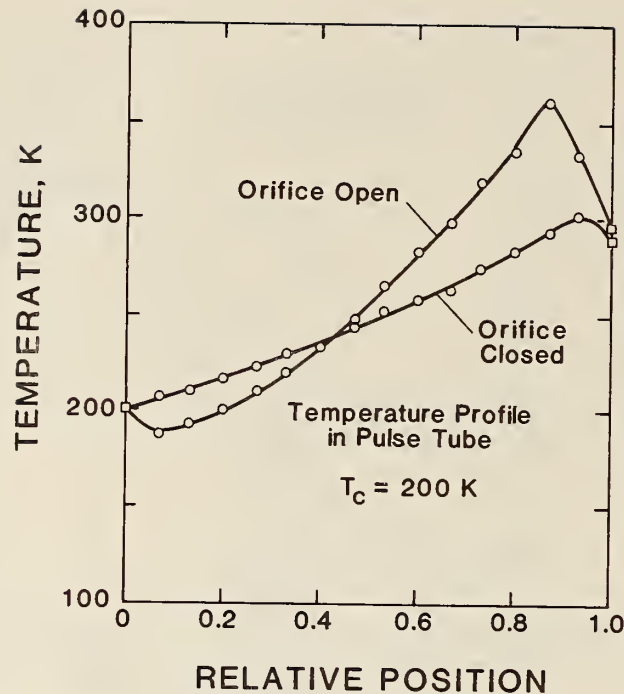
Figure 3–8.   Comparison of average temperature profiles in the tube with the orifice open and the orifice closed.

order to show that the profiles all have basically the same shape, a normalized temperature was plotted as a function of position for each case in figure 3–9.

The theoretical and experimental temperature oscillations at different points in the pulse tube are presented in figure 3–10. The theoretical oscillations were calculated using eq (2–32) and show the sinusoidal behavior assumed in the model. The temperature amplitude predicted by the model basically increases linearly from the cold end to the hot end. However, the experimental temperature exhibits a large amplitude at the center of the tube with much smaller amplitudes at the ends. This behavior is attributed to the isothermal heat exchangers which fix the end temperatures. The oscillation at the cold end in figure 3–10a has very broad peaks with amplitudes less than half of those of the theoretical oscillations. The oscillation at the hot end in figure 3–10a has maxima with sharp peaks with about the same magnitude as the sine oscillation, while the minima are much flatter. The temperature oscillation for the center in figure 3–10b shows considerable deviation from sinusoidal behavior with sharp maxima and broad minima.
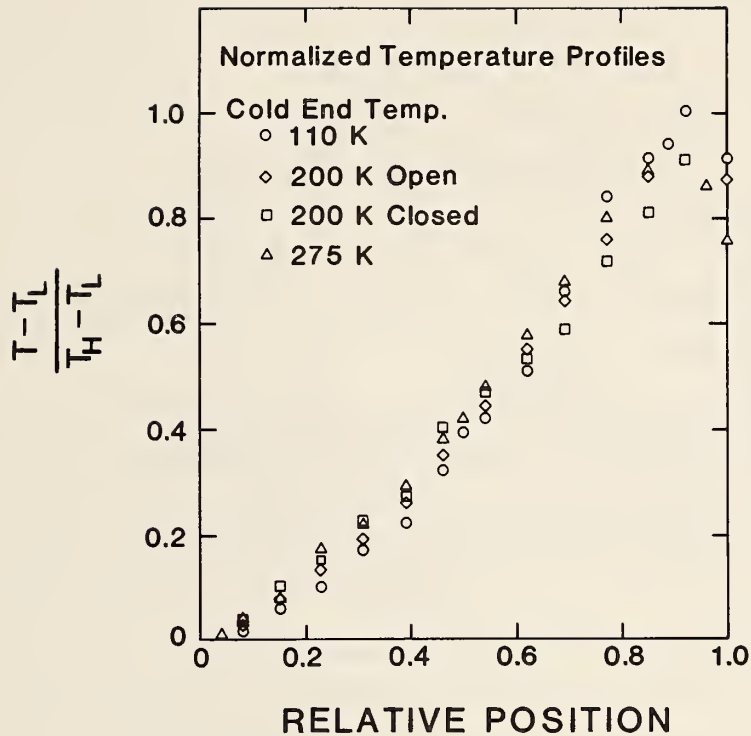
Figure 3–9.   Normalized temperature as a function of position in the
pulse tube where T_L and T_H are the low and high values
respectively of the data set.

The temperature oscillation at the center of the tube is also shown in figure 3–10b
for operation with the orifice closed. Theory predicts that the amplitude for this case will
be slightly smaller than for the case with the orifice open since the average temperature
and the temperature gradient are smaller. The experimental amplitude for operation with
the orifice closed is about four times smaller than that with the orifice open.
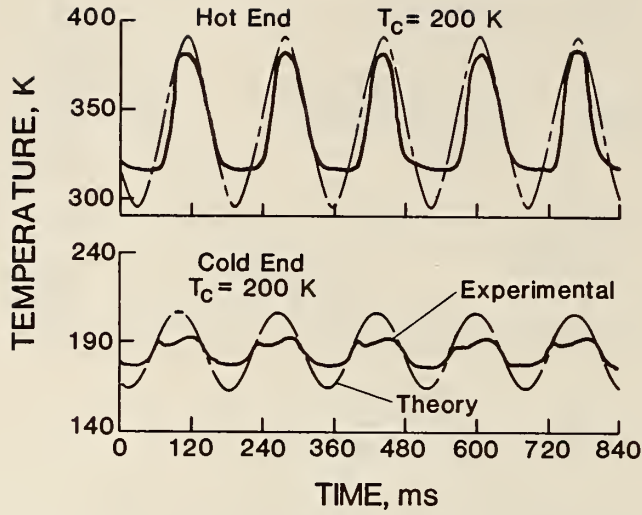
(a)
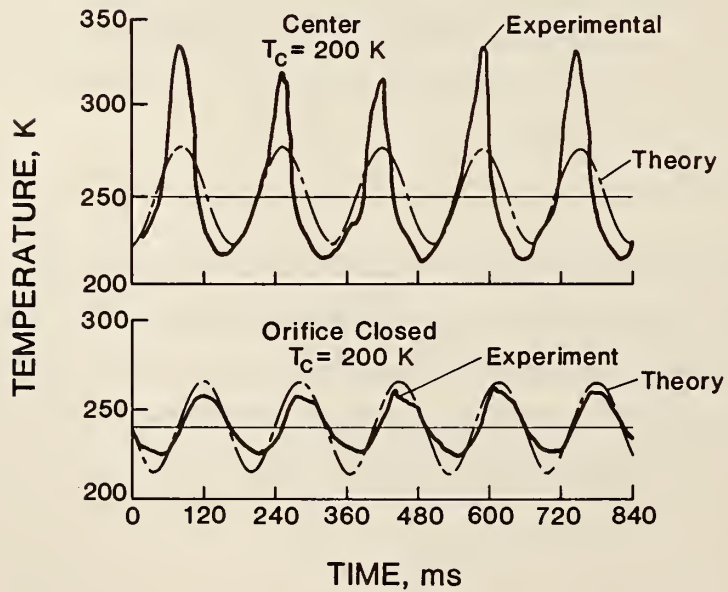
(b)

Figure 3–10.   Comparison of experimental temperature oscillation with theoretical sine oscillation at (a) cold and hot ends with orifice open, and (b) center of tube with orifice open and orifice closed.

CHAPTER 4

DISCUSSION OF RESULTS

4.1   Assumptions in the Model

In this analytical development, several basic assumptions are used to simplify the analysis. Some of these assumptions are very good for typical pulse tube systems while others place some serious limitations on the resulting enthalpy flow equations. A comparison of theoretical and experimental values of refrigeration power reveals that values calculated from Model 1 (eq (2–40)) are between 3 and 6 times greater than gross refrigeration measurements. Figure 4–1 shows a plot of the ratio of theoretical to experimental refrigeration power as a function of cold–end temperature. Similar plots are shown for Model 2 (2–50) and Model 3 (2–63), in figures 4–2 and 4–3. The ratio of theoretical to experimental values for the model which neglects dead volume is between 8 and 12 while the ratio for the model which accounts for the effect of dead volume is between 3 and 6. After the various assumptions in the model are examined, an explanation is offered for the difference between the experimental and theoretical values of refrigeration power.
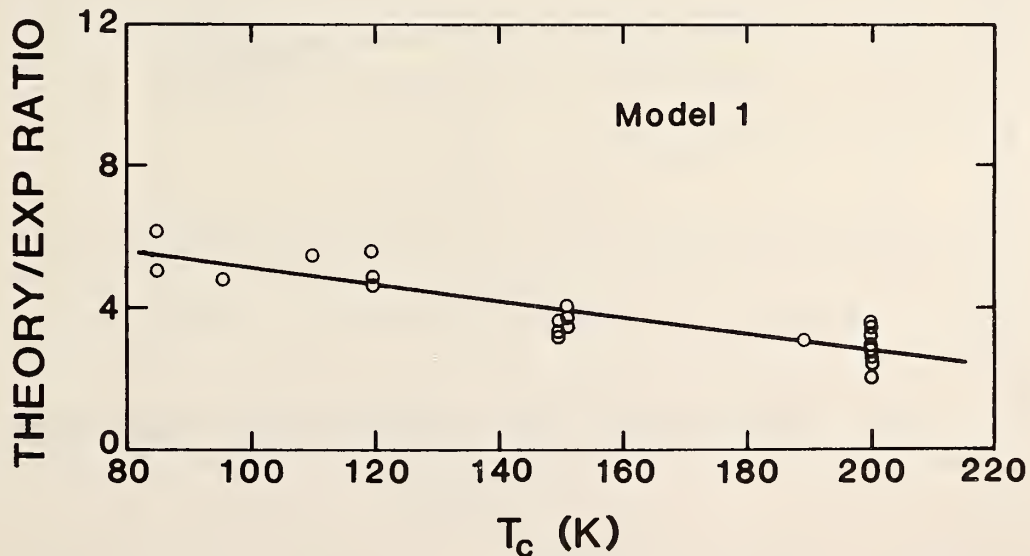

Figure 4–1.   Ratio of theoretical refrigeration power to experimental values as a function of cold–end temperature for $<\dot{H}>/<\dot{M}_c>RT_c$.

Best–fit lines are plotted in figures 4–1, 2, and 3 to show the general trend of increasing divergence of the theoretical and experimental values with decreasing temperature. The uncertainty in the refrigeration power ratios is ±7%.

The first assumption made in the model is that the working fluid is an ideal gas. The typical gas used in the pulse tube is helium, which behaves ideally at temperatures above 50 K. Ideal behavior is expected for the system in this work since temperatures below 100 K are not encountered. The next assumption made is that the pressure oscillation is a function of time only. This simplification is valid in this case since the pulse frequencies used were not high enough to cause pressure fluctuations along the tube. The model also describes a system at equilibrium, which means that both the cold–end temperature and the average temperature gradient in the tube are assumed to be constant. These conditions would not exist during system cool–down.

The assumption of an adiabatic tube makes the model specific to the orifice pulse tube. The absence of heat transfer between the gas and the tube wall means that cooling occurs only due to expansion in the tube from flow through the orifice, and that entropy is constant in the tube. This is the ideal case for the OPTR since heat transfer can actually be detrimental to performance [23]. With operation at relatively high frequencies and a
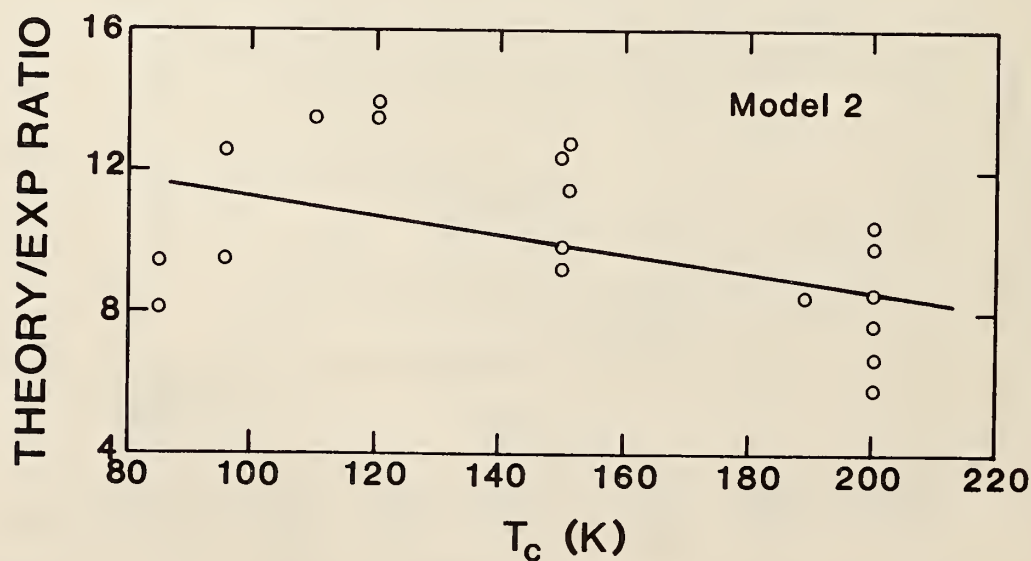

Figure 4–2.   Ratio of theroretical refrigeration power to
                   experimental values for the model neglecting dead volume.
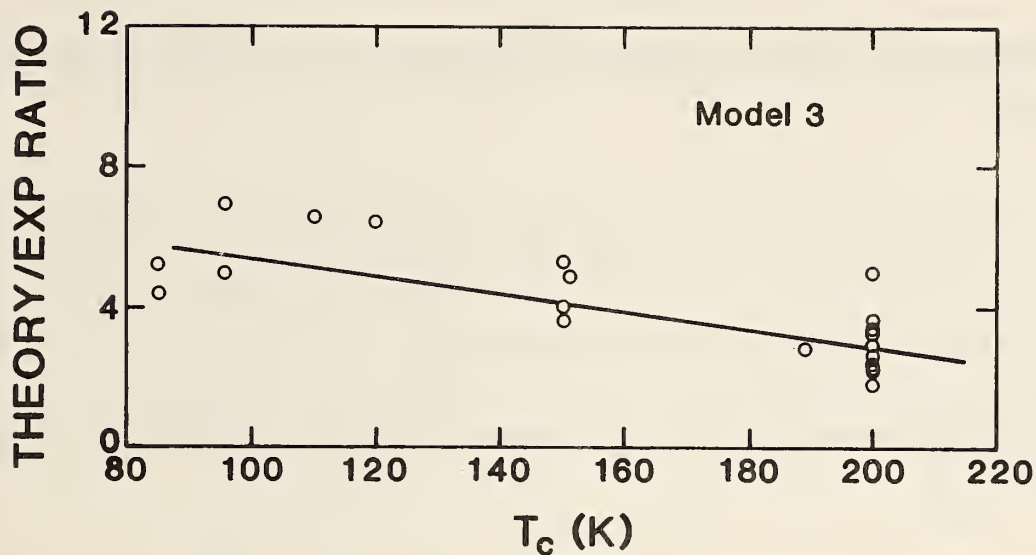
Figure 4–3.   Ratio of theoretical refrigeration power to experimental values for the model accounting for dead volume.

large tube diameter, the adbiatic assumption is reasonable since the thermal penetration depth is proportional to $1/\sqrt{\nu}$. For a system with helium at 300 K and operating at 6 Hz, the thermal penetration depth is about 1 mm. The thermal penetration depth assuming a flat plate is $\gamma = 1/\sqrt{\pi \rho C_P \nu}$. This value is small compared to the 10 mm radius of the tube used in this work. Therefore, the assumption of an adiabatic tube is appropriate for the system.

The most important simplification in the model is the assumption of sinusoidal behavior for the pressure oscillation. This assumption means the temperature and mass flow rate are also sinusoids. The mathematics is then greatly simplified and phasor analysis can be used to describe the oscillations. In the real system, the volume variation in the compressor is the true sinusoid and not the pressure which varies as $1/V$. However, for small compression ratios ($P_d/P_a \ll 1$), the pressure approaches a sinusoidal behavior. In the test apparatus, compression ratios of up to $P_d/P_a = 0.44$ were observed, which is probably the upper limit for small P_d/P_a. Therefore slight deviation from a sine oscillation was expected and was observed for the experimental pressure. The pressure oscillation had a sharper peak than a pure sine oscillation which contributes to the decrease in magnitude of the experimental enthalpy flow. However, the behavior of the pressure oscillation affects

only the magnitude and not the dependencies of the enthalpy flow on the different parameters.

Since there is significant dead volume of about 50 cm³ in the test apparatus, the model which assumes no dead volume is not very realistic. A comparison of Figures 4–2 and 4–3 gives an indication of the effect of dead volume on the performance of the pulse tube. The model which neglects dead volume predicts an enthalpy flow more than two times greater than the model which accounts for dead volume. Data from the gross refrigeration measurements as well as the calculated values from the models are shown in Appendix B.

Probably the most limiting assumption in the model is that the tube is infinitely long; therefore neglecting end effects. The sinusoidal behavior of the various oscillations as discussed above is actually valid only for the center of the tube. The temperature at the ends of the tube are fixed by the isothermal heat exchangers, which flatten the oscillation, and cause a significant deviation from sinusoidal behavior. The end effects are noticeable in a comparison of the experimentally measured temperature oscillation with the sine oscillation predicted by theory in figure 3–10a. The smaller experimental amplitudes at the ends contribute to the difference between the theoretical and experimental refrigeration power.

Since the enthalpy flow in the model is the gross refrigeration power (as shown in the development of the energy balance eq (2–5)), assumptions neglecting losses such as those due to conduction, heat leaks, or regenerator ineffectiveness are not necessary.

4.2   Describing the Refrigeration Process

From the experimental measurements of the temperature oscillation, two very useful plots which characterize the OPTR can be constructed . The first plot, presented in figure 4–4, shows the average temperature profile in the tube along with experimental and theoretical profiles of the dynamic temperature. The solid line follows the plot of the experimental time–averaged temperatures in the tube for $T_c = 200$ K; the slope is very steep for operation with the orifice open. The broken lines represent temperature amplitudes for the system according to eq (2–32) of the model. The dashed lines show the experimental amplitudes. As observed before, the actual amplitude above the average temperature is very large in the center of the tube, much larger than predicted by theory.

Below the average temperature, the theoretical curve nearly matches the actual values.
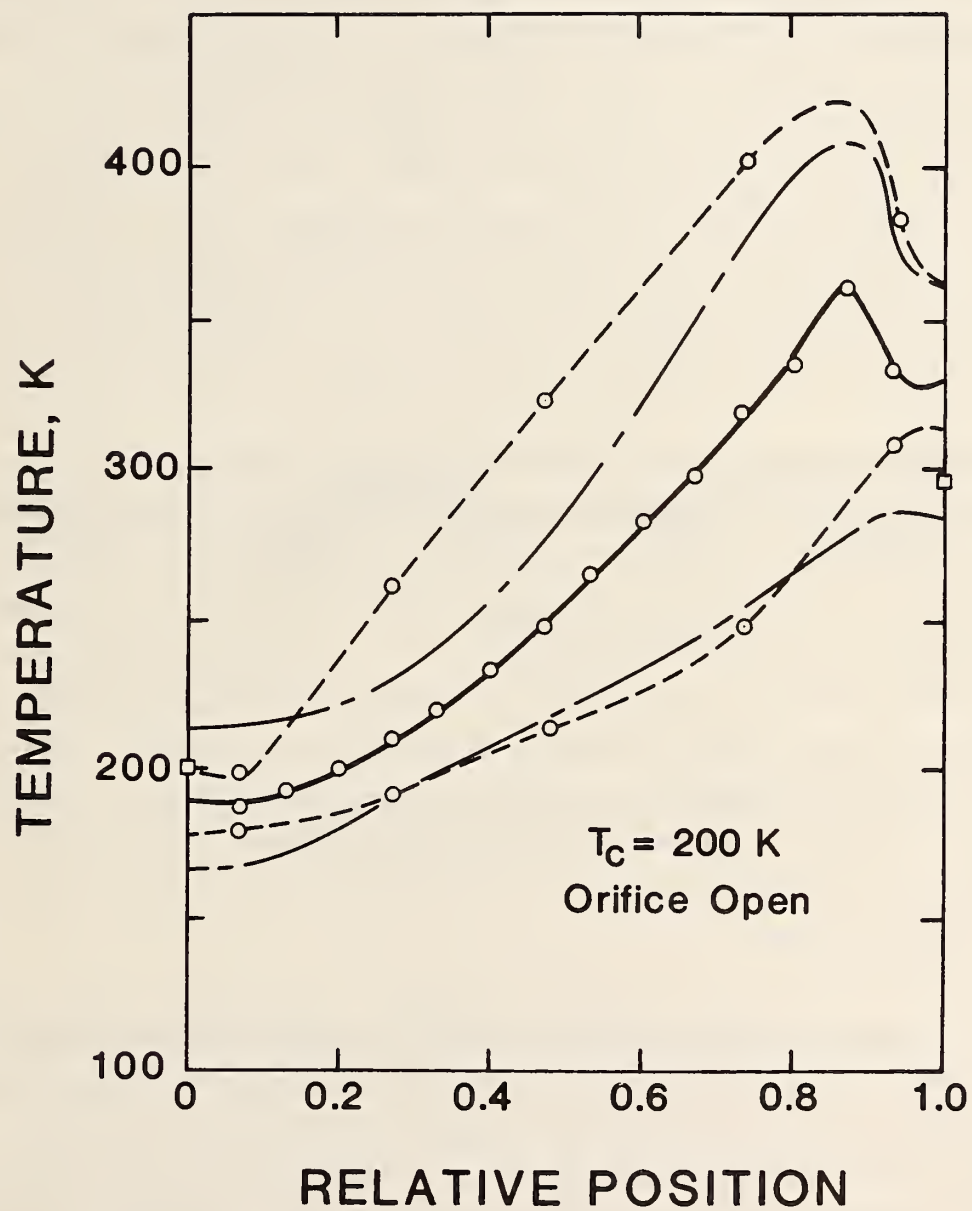

Figure 4–4.   Comparison of dynamic temperature profiles to
                   the average temperature profile.

The large dynamic temperature and the steep average temperature profile can be explained by looking at the gas in the tube center. Due to the motion of the piston, gas in this region moves back and forth but does not leave the tube. As the gas moves, the temperature gradient moves with it, alternately moving gas at the hot–end temperature and then gas at the cold–end temperature to the middle of the tube. The greater gas displacement with the orifice open than that with the orifice closed explains the steeper temperature gradient observed in the OPTR as compared to the BPTR. It is understandable then why there exists an optimum orifice setting in the OPTR. The larger the orifice, the greater the expansion of gas in the tube. However, if the orifice is too large, gas will travel the entire length of the tube and the temperature gradient will deteriorate. In effect, the quantity of gas in the center of the tube acts as a buffer between the two ends preserving the temperature gradient. The buffer gas in the OPTR tube seems to act as a "gas displacer" and to play a role very similar to the displacer in the Stirling refrigerator.

The second plot using the experimental temperature oscillation is shown in figure 4–5. Gas temperature is plotted against the mass of gas moved in the tube. The three cases displayed here are for the cold end, the hot end, and the center. This figure is referred to as a T–m diagram and is analogous to the P--V diagram commonly used to study thermodynamic systems. Just as the area in a P–V diagram represents the work per cycle in a system, the area in a T–m diagram represents the enthalpy transported per cycle. Figure 4–5 gives a good description of enthalpy flow in the OPTR. The enthalpy flow at the cold end is characterized by a large amount of mass with a very small dynamic temperature. Enthalpy flow in the center of the tube is due to a smaller amount of gas but with a very large temperature amplitude. The hot end has the least mass transported with intermediate temperatures.

At this point, an attempt is made to describe the refrigeration process in the PTR in both a physical and a thermodynamic sense. The BPTR and the OPTR operate on similar thermodynamic cycles. The process consists of heating due to adiabatic compression, a shift in phase between the mass flow rate oscillation and the temperature oscillation, and then cooling due to adiabatic expansion. The experimental temperature measurements, however, have shown that there is a significant difference in the average and dynamic temperature profiles in these two refrigerators. Also, the difference leads to greater refrigeration power in the OPTR. Figure 4–6 shows the temperature as a function of position in the tube to help illustrate the difference in the refrigeration process. The difference is in the method of phase shift. The BPTR relies on heat transfer to the tube
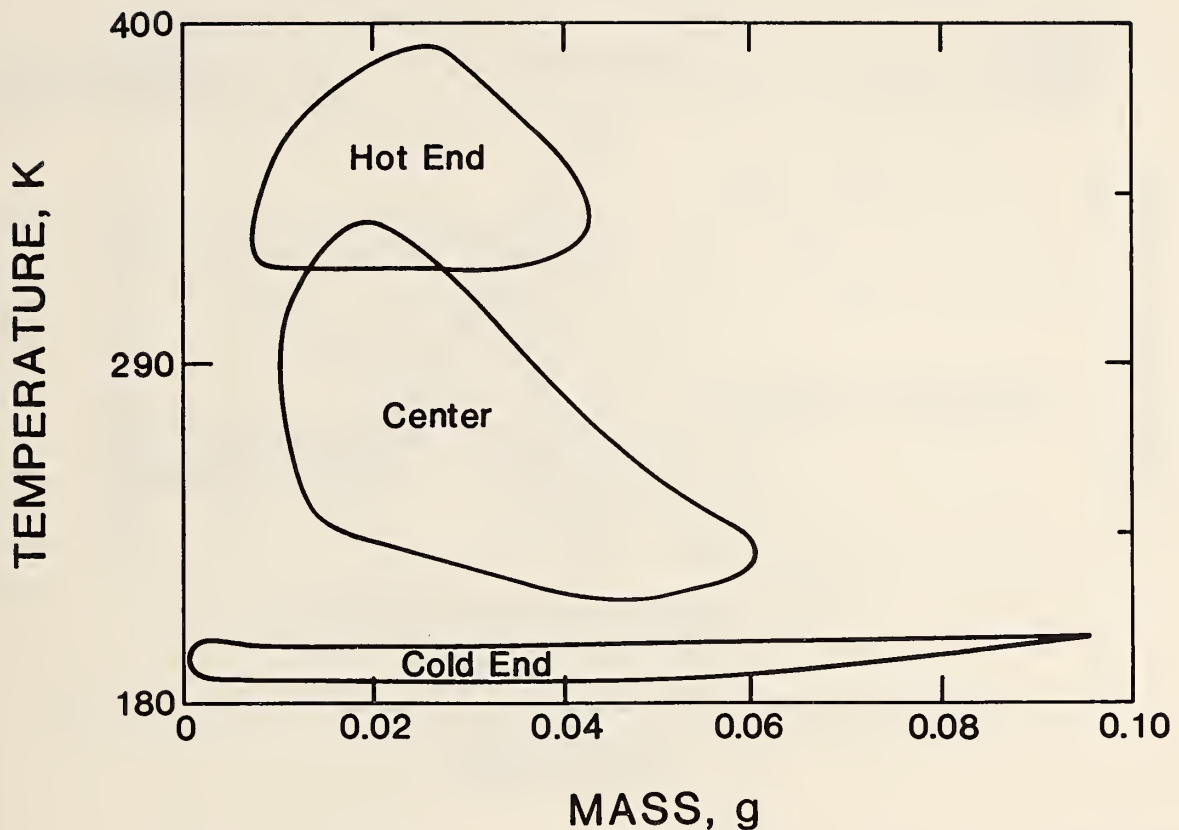
Figure 4–5.   T–m diagram characterizing enthalpy flow at the hot end,
                center, and cold end of the pulse tube.

wall to cool the gas after the compression phase while the OPTR relies on the expansion of
gas in the tube due to flow through the orifice to cool the gas. The cooling and therefore
the phase shift in the BPT are limited to the temperature of the tube wall. Figure 4–6
shows how the gas in the OPT can be cooled below the wall temperature (2–3). During
flow through the orifice back into the tube (4–6), the gas is heated above the wall
temperature. This behavior is confirmed experimentally by the large dynamic
temperatures seen in figures 4–2 and 3–10b. The larger temperature amplitudes generated
by the orifice result in a larger enthalpy flow. In figure 4–6 the greater area enclosed by
the path on the left explains qualitatively why refrigeration power is greater in the OPT.
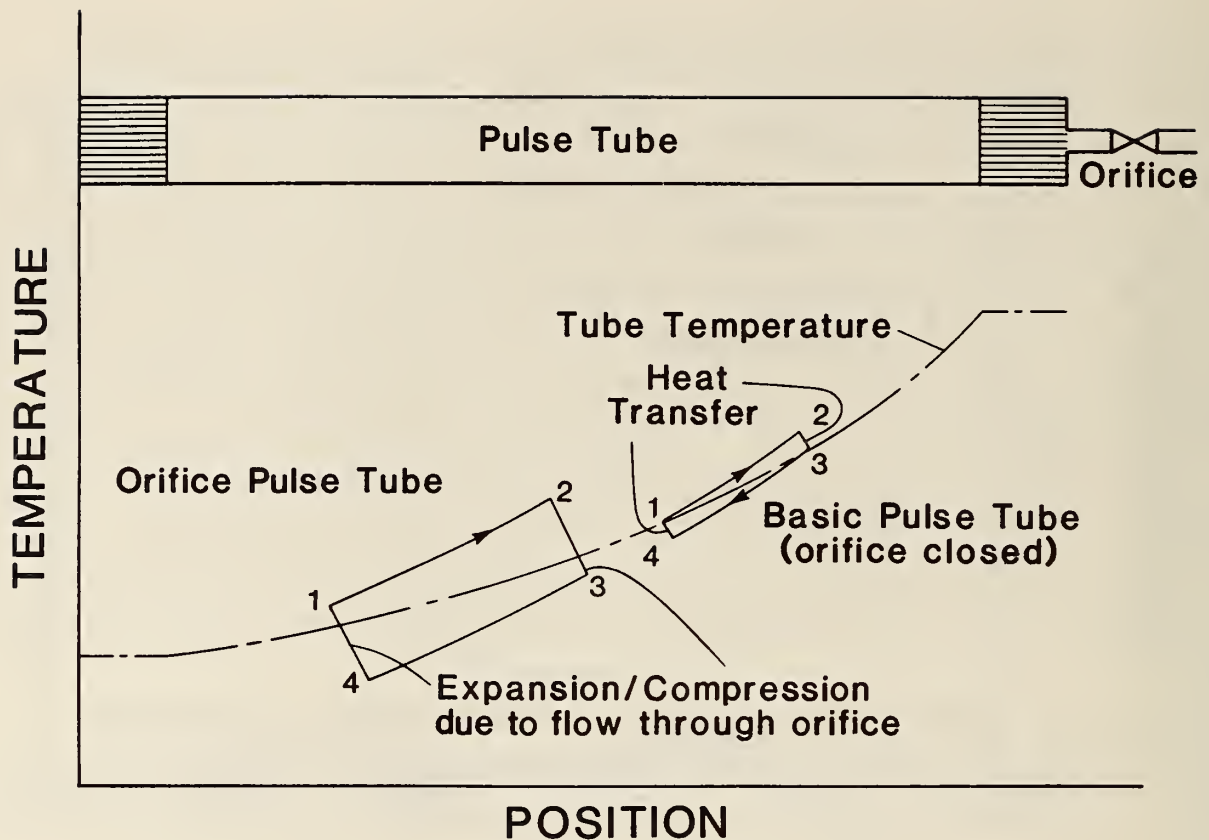
Figure 4–6.   Temperature as a function of position for an element
of gas in a pulse tube with the orifice open and with
the orifice closed.

Another method of describing the refrigeration process in the orifice pulse tube
involves a T–S diagram. It is impossible to represent pulse tube refrigeration on a T–S
diagram in the traditional sense since each element of gas in the system follows a different
path. For example, the buffer gas in the center of the tube traces out a simple vertical line
on the T–S diagram since it experiences only the constant entropy processes of adiabatic
compression and expansion. The gas which moves in and out of the ends of the pulse tube
is more interesting. Figure 4–7 shows a T–S diagram for an element of gas which enters
and leaves the cold end of the tube. Starting in the compressor at point 1 in the figure, the
gas is cooled to the cold end temperature as it is moved by the piston through the
regenerator and the cold end heat exchanger (1–2). The gas then experiences adiabatic
compression in the tube and follows path (2–3). At this point, the gas in the OPTR
follows path (3–4) and is cooled by adiabatic expansion due to flow of other gas elements
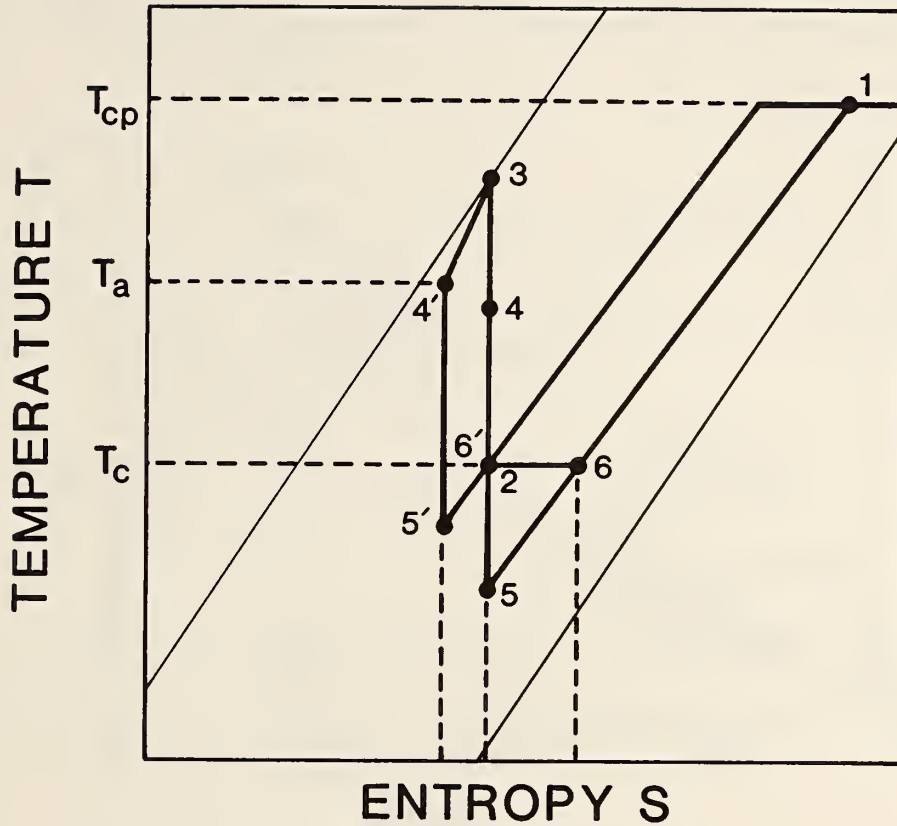
62

Figure 4–7.   T–S diagram representing the thermodynamic
                     cycle of an element of gas at the cold
                     end of the tube.

out the orifice and into the reservoir. The path corresponds to path (2–3) on the T–x
diagram in Figure 4–6 where gas moves toward the hot end as it cools below the average
temperature. In the BPTR, however, cooling occurs at constant volume (3–4'), due to
heat transfer with the tube wall and is limited to the wall temperature. The piston then
moves gas back toward the cold end and the element of gas cools adiabatically from 4 to 5
in the OPTR and from 4'to 5' in the BPTR. The gas flows back through the cold–end
heat exchanger and heat is absorbed at constant pressure along the paths (5–6) and
(5'–6'). The gas completes the cycle back at point 1 in the compressor. The area under
the curves (5–6) and (5'–6') represent the refrigeration power generated in the OPTR and
BPTR, respectively. Just as shown in the T–x diagram in figure 4–6, the area is greater
for the OPTR than for the BPTR.
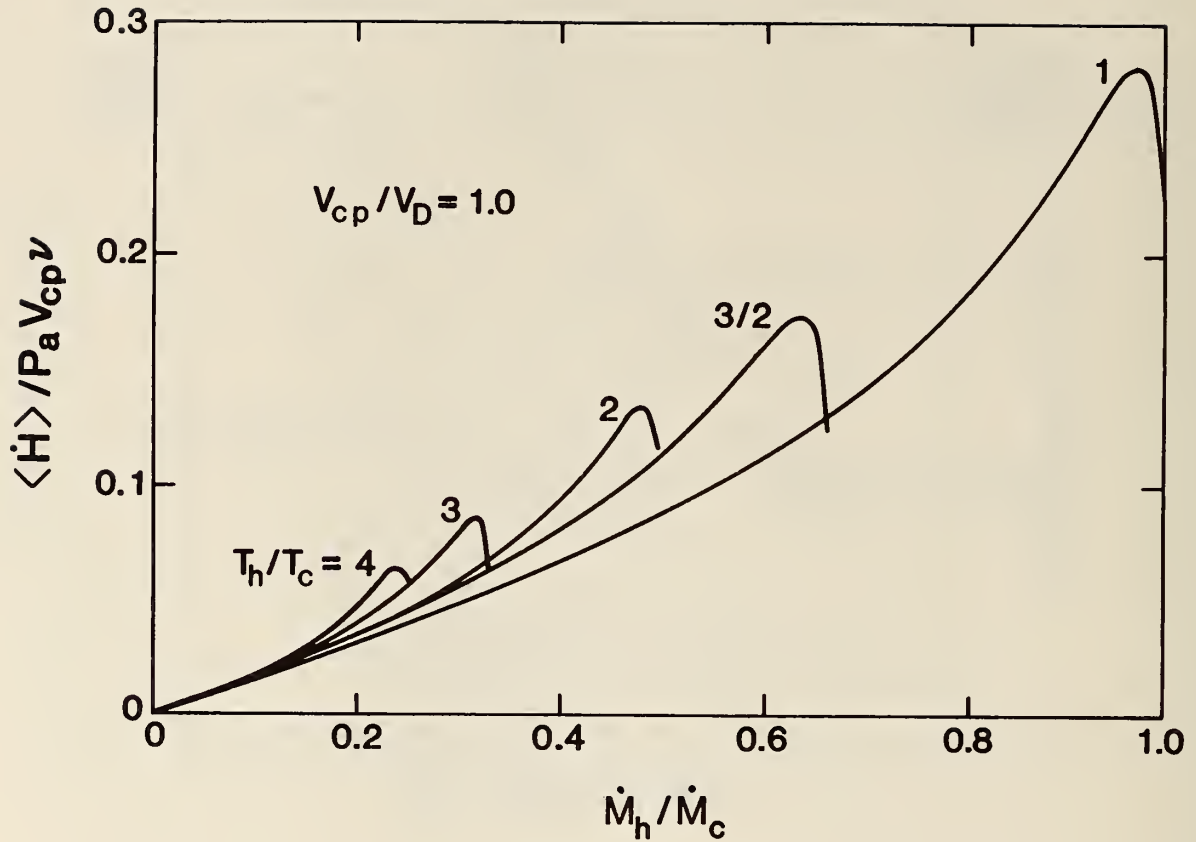
Figure 4–8.   Gross refrigeration power as a function of
mass flow ratio for different temperature
ratios (T_h = 350 K).

If the theory of operation described above in figures 4–6 and 4–7 is correct, we will find that heat transfer in the OPTR is detrimental to performance. That is, heat transfer would limit the dynamic temperature in the OPTR and decrease refrigeration capacity. This is exactly the behavior observed by Radebaugh and Herrmann in their 1986 work. They showed that the OPTR operated better at high frequencies where heat transfer is insignificant [23]. Also, in this work, a significant loss of performance in the OPTR was observed when the temperature probe was inserted into the tube. The farther the probe was inserted, the greater the loss of refrigeration power. (See data in Appendix B) The loss of performance is attributed to the increase in heat transfer area.
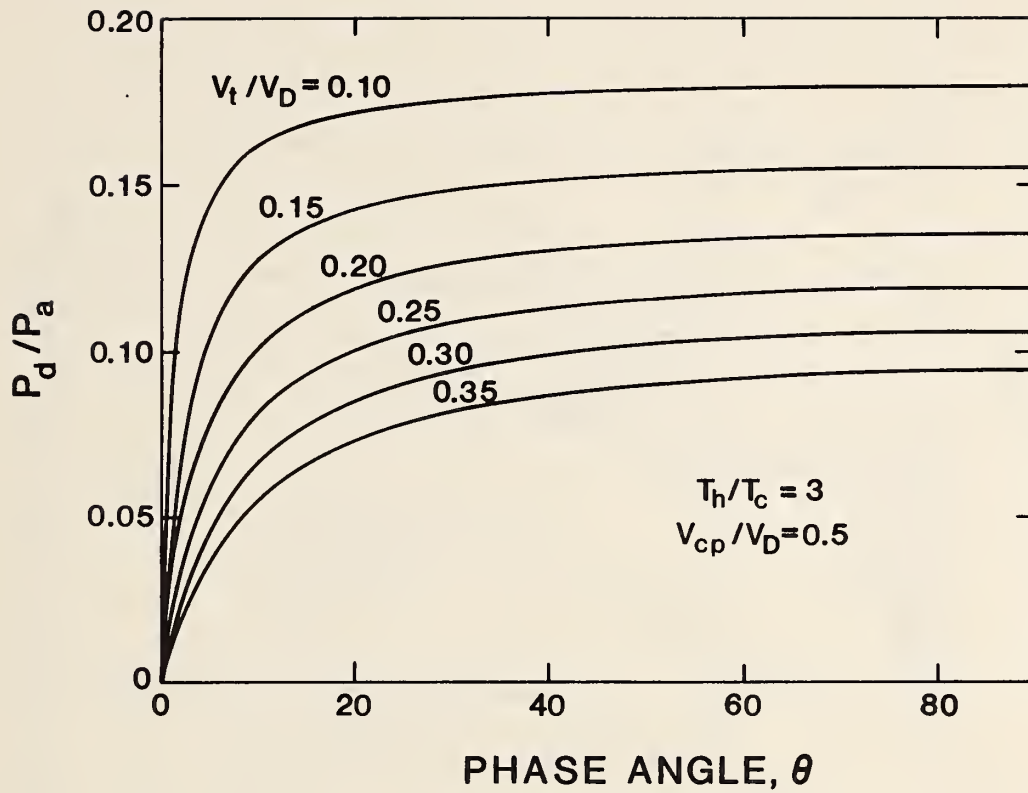
(a)
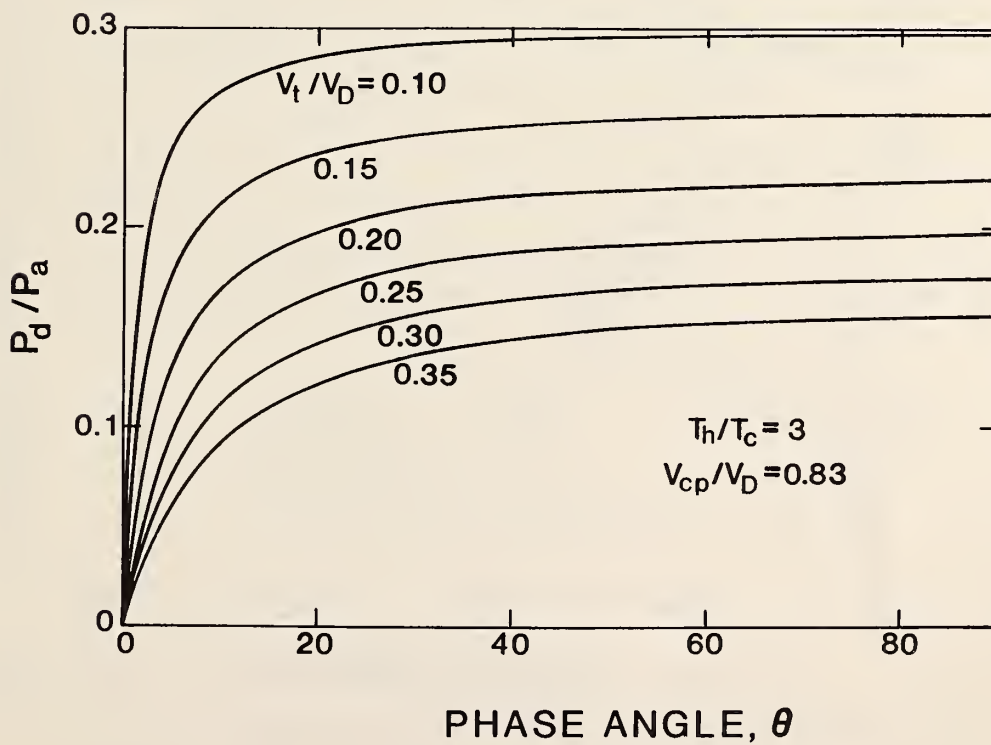
(b)

Figure 4–9. The effect of mass flow through the orifice on pressure ratio.

(c)

(d)

Figure 4–9.

Figure 4–10a.   Gross refrigeration power as a function of
pulse tube volume for six different compressor
sizes and four different cold end temperatures
(T_h = 350 K).

67

Figure 4——10b

68

Figure 4–10c

69

Figure 4–10d

70

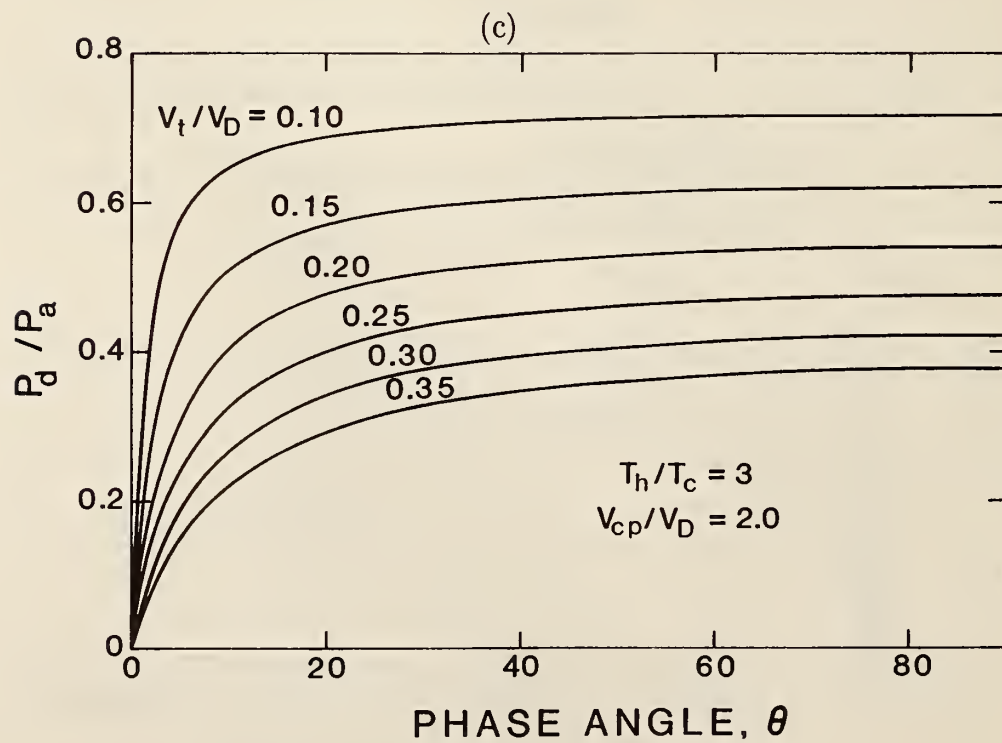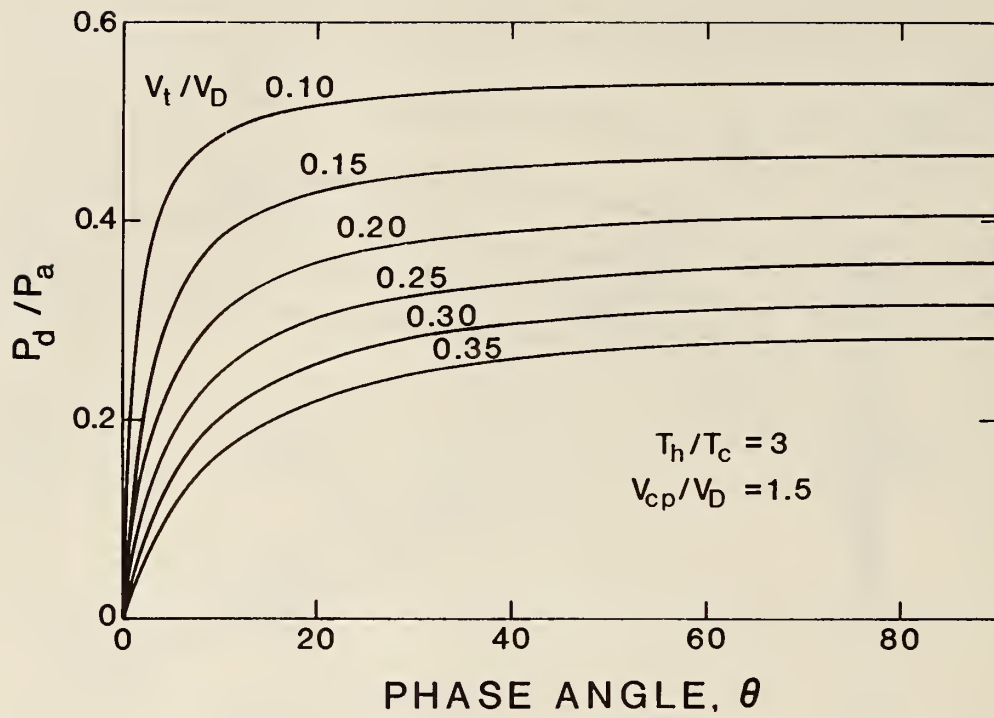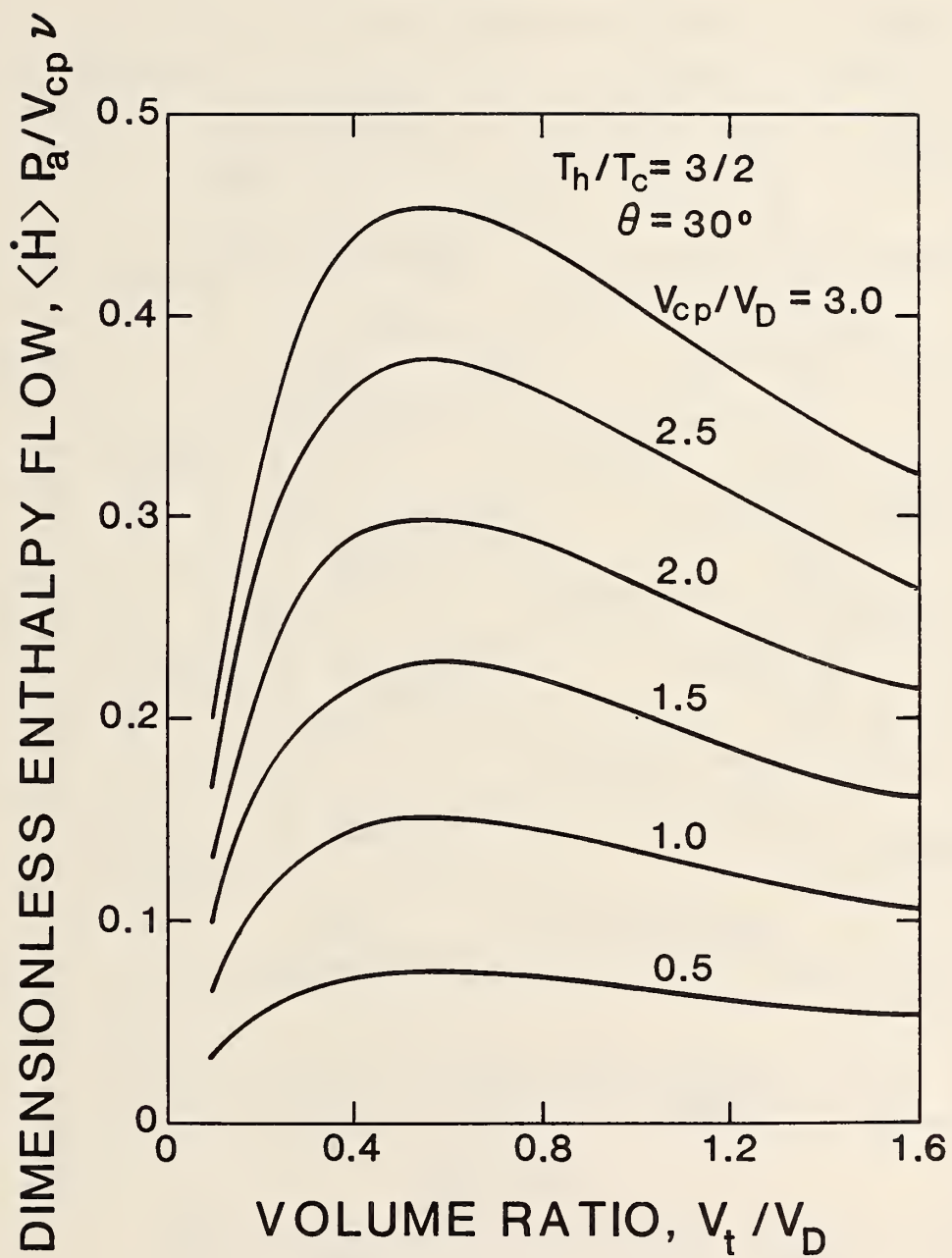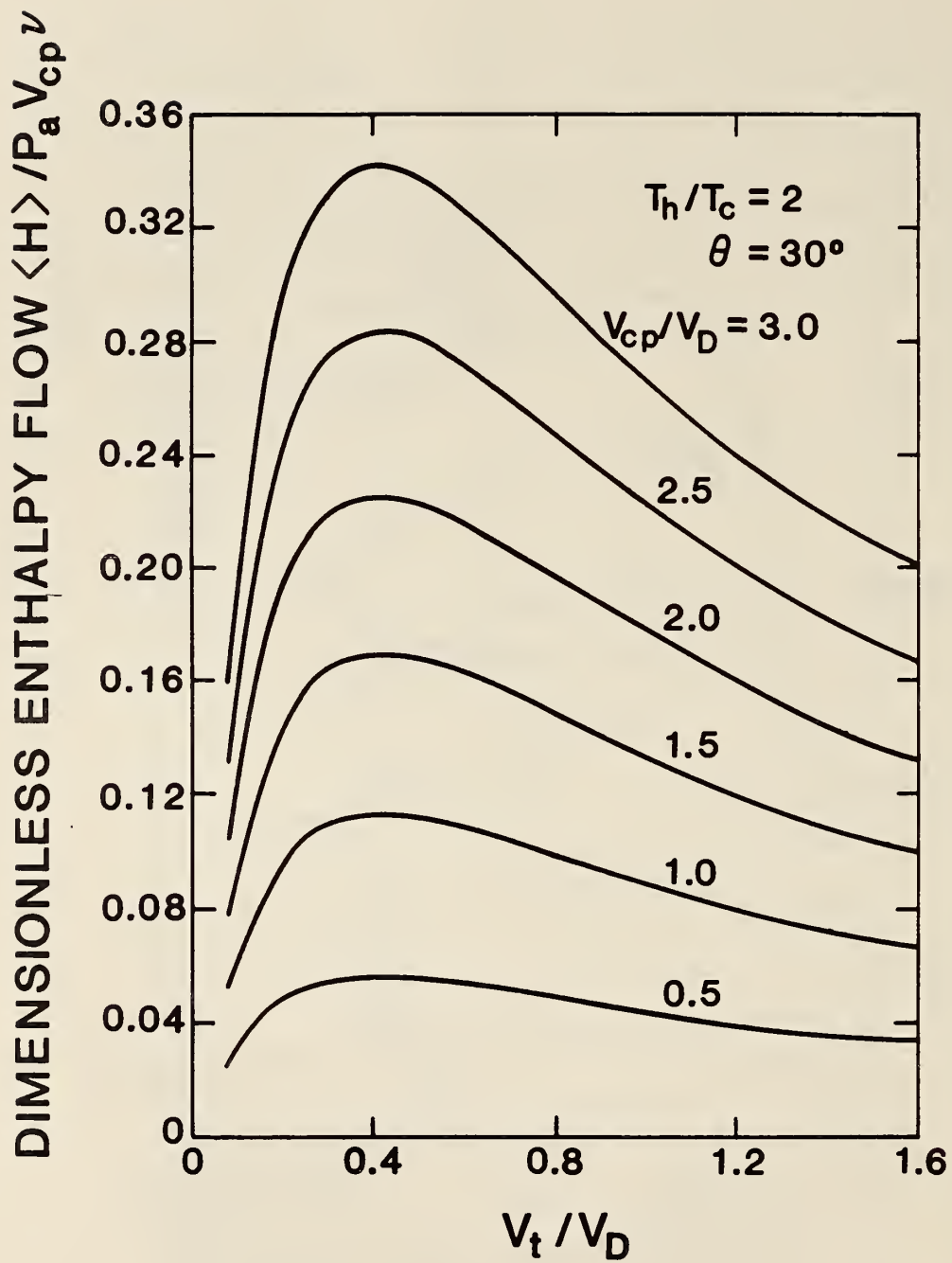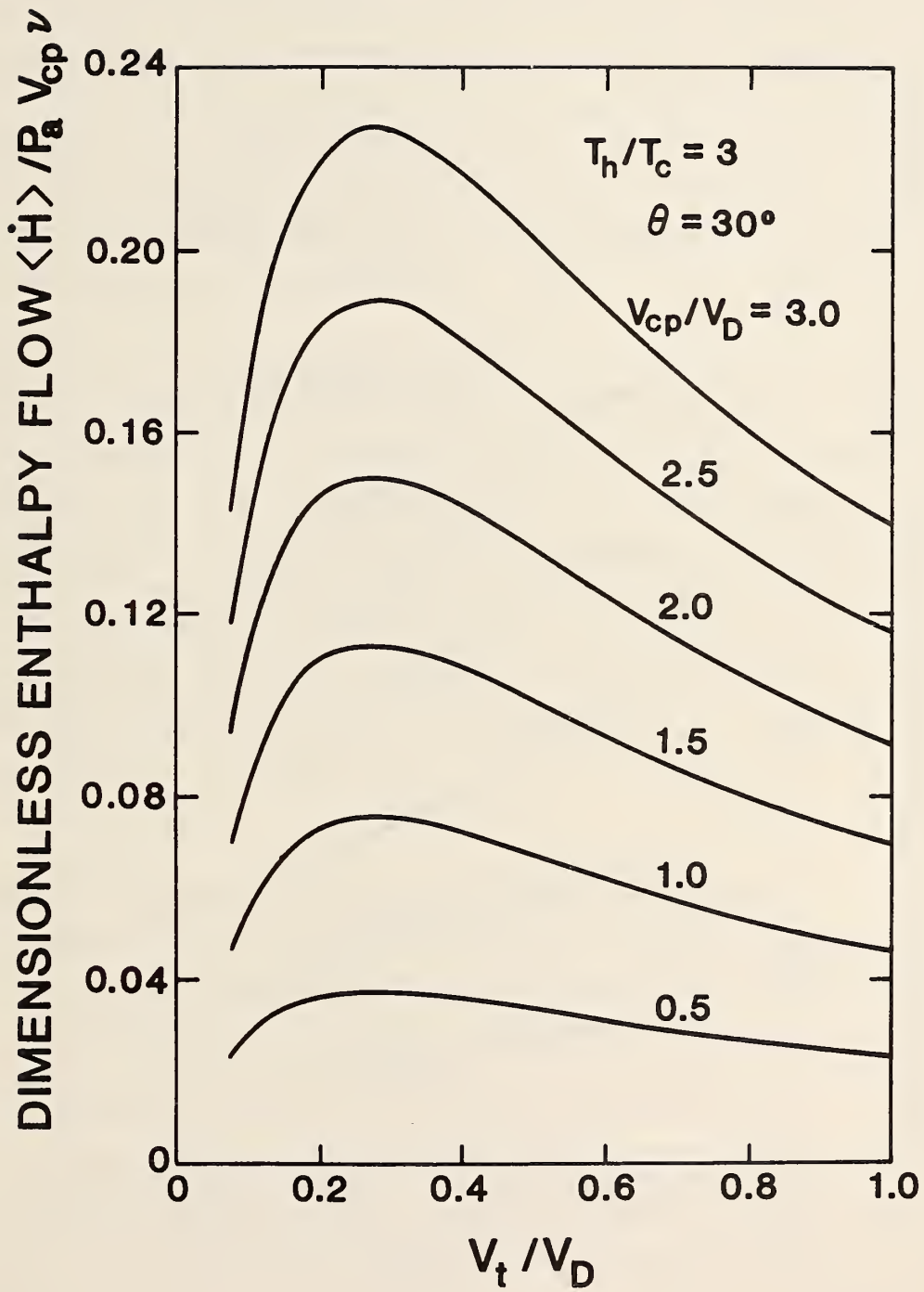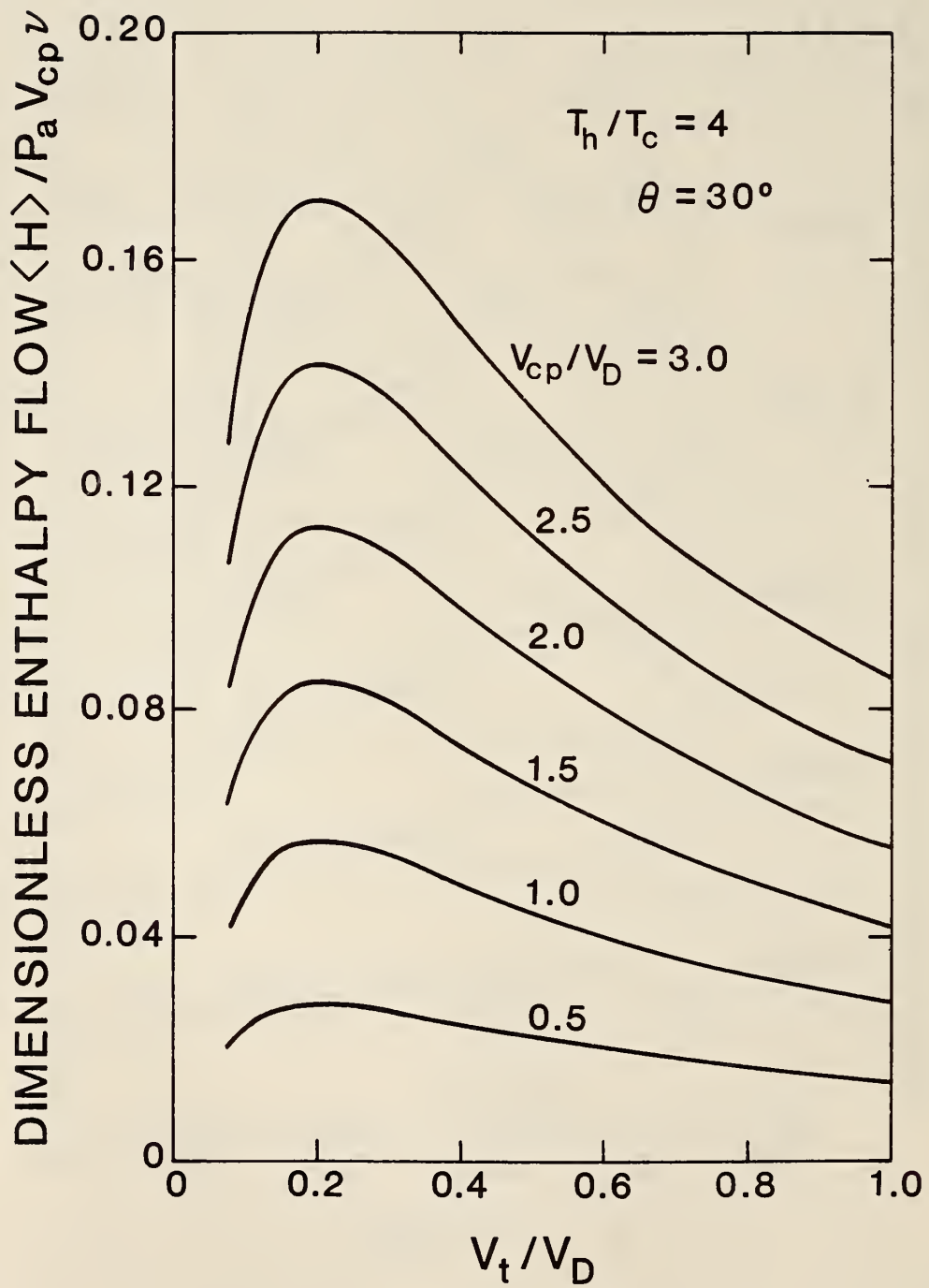## 4.3   Optimizing the Orifice Pulse Tube Refrigerator

For design the most useful expression resulting from this analytical study is eq (2–64). This equation is written in terms of important design parameters including compressor swept volume, pulse tube volume, dead volume, average pressure, pulse frequency, and mass flow rate through the orifice or phase angle θ. We must realize, though, that this equation describes only the pulse tube itself and does not account for the effect of regenerator parameters on the optimum pulse tube configuration. An effort to determine the optimum relationship between regenerator and pulse tube volumes was conducted by Chowdhury and Radebaugh [26].

Figure 4–8 shows dimensionless enthalpy flow from eq (2–66) as a function of mass–flow ratio for different cold–end temperatures. The gas temperature at the hot end (T_h) was approximately 350 K for this system. For a given temperature ratio, refrigeration power increases as flow through the orifice increases due to the expansion of gas in the tube. However the effect of the expansion is offset by a decrease in the compression ratio P_d/P_a, and a maximum in refrigeration power results. The point at which the maximum occurs is the optimum mass–flow ratio and depends on the temperature ratio and the ratio of pulse tube volume to dead volume. Of course the magnitude of the maximum is a function of the compressor size or V_{CP}/V_0. For figure 4–8,

$$V_{CP}/V_0 = 1.$$

The effect of mass flow through the orifice on the pressure ratio is displayed in figure 4–9. This series of plots for different compressor sizes (V_{CP}/V_0) and pulse tube sizes (V_t/V_0) show P_d/P_a as a function of phase angle θ. When the orifice is closed, $\theta = 90°$ and P_d/P_a is at a maximum. As the orifice is opened, $\dot{M}_h/\dot{M}_c$ increases while θ and P_d/P_a decrease. Plots 4–9a through 4–9d can be used to predict the approximate pressure ratio obtained in a given pulse tube system for $T_h/T_c = 3$. The curves in these plots, constructed from eq (2–60), predict values of P_d/P_a about 5 times greater than experimental measurements. The expression for P_d/P_a which neglects dead volume, eq (2–47), predicts values about 10 times greater than experimental measurements.

Another important series of plots is shown in figure 4–10. Dimensionless enthalpy flow from eq (2–64) is plotted versus the volume ratio V_t/V_0 for six different values of

$_{CP}$/V_D and four different cold end temperatures. These plots show a maximum in refrigeration power and the optimum pulse tube volume can be determined for a given compressor size, dead volume, and cold end temperature. For comparison, the optimum V_t/V_D for T_C = 80 K (T_h/T_C = 4) predicted by the model is 0.22 while the experimental ratio was 0.20 [26]. This experimental ratio was calculated using the pulse tube system in reference [26]: regenerator IV with V_t = 7.35 cm³ and T_C = 81 K.

The plots shown in figures 4–10a through 4–10d can be constructed for different values of phase angle θ. The model, however, predicts that the maximum refrigeration power occurs in the limit as the phase angle θ and pulse tube volume V_t approach 0. In the context of the model, this result is reasonable. The maximum expansion in the tube occurs when $\theta = 0$ and the maximum pressure ratio occurs when V_t = 0. However, lower limits on pulse tube volume and orifice opening size are defined for a real system by the need to preserve the temperature gradient in the tube. As explained previously, performance decreases when the so–called buffer gas leaves the tube, which occurs if the tube volume is too small or the phase angle is too small. The optimum phase angle for any pulse tube system was determined to be 30° from the experimental data shown in the Appendix B.

One important point to keep in mind when applying the curves in figure 4–10 is that the value of V_D is dead volume at ambient temperature. Dead volume which exists at the cold end of a system must be corrected for temperature to obtain a realistic value of V_t/V_D .

CHAPTER 5

CONCLUSIONS

The analytical study presented here has contributed to our understanding of the refrigeration mechanism and the capability of the pulse tube refrigerator. We have learned that there are significant differences between the mechanism of the OPTR and the BPTR. Heat transfer between the tube wall and the fluid is undesirable in the the OPTR since it degrades the dynamic temperature and therefore the gross refrigeration power. The BPTR, however, relies on heat transfer to create the heat pumping effect. Clearly, flow through the orifice generates greater refrigeration power and gives the OPTR more potential for practical application that the BPTR.

The energy balance used in this analytical development reveals that both net and gross cooling power can be measured in the PTR unlike other cryocoolers, . We have also learned that the enthalpy flow analysis and the use of phasors are convenient and effective methods of analyzing pulse tube systems. This approach can be generalized and should be a useful tool for the study of other regenerative refrigerators.

An obvious test for validity of an enthalpy flow analysis is conservation of energy. The enthalpy equations generated in this work satisfy this requirement since they predict constant enthalpy flow along the adiabatic tube.

Experimental results also support the validity of the model. The dependence of refrigeration power on average pressure, pressure ratio, frequency, and mass—flow ratio predicted by the model matches experimental data. Furthermore experiments and the model agree that helium produces the best performance when used for the working fluid for the OPTR.

The refrigeration powers predicted by the model, however, are at best 3–6 times greater than experimental measurements. The difference is attributed to the simplifying assumptions made in the derivation of the model in order to obtain closed solutions. These assumptions include laminar flow in the pulse tube as well as through the orifice, sinusoidal variations in pressure, temperature, and mass flow rate, and an infinitely long tube. In order to improve the analytical model and our understanding of the OPTR, further experimental investigation is required. One recommendation for such work is a study to

characterize flow in the pulse tube to determine the effects of turbulence due to oscillating flow and a tube of finite length.

The result of including dead volume in the enthalpy flow analysis is an increase in the complexity of the equations and a factor of 2 decrease in the refrigeration power predicted by the model. Dead volume is therefore an important parameter to consider in the design of PTR systems.

The refrigeration power measurements taken in this work are consistent with previous results. For example, at 200 K with a pulse tube volume of 30 cm^3, a gross cooling power of 34 W and an efficiency of 17% of Carnot efficiency were measured. These values match results reported by Herrmann and Radebaugh in 1986 [23].

The plots generated from the model and presented in Chapter 4 are useful for approximate design of an OPTR system. The system described here consists only of the pulse tube itself. The regenerator is treated only as dead volume in the system. Before an overall system can be effectively designed and optimized, the relationship between the regenerator and pulse tube volume must be more clearly understood.

ACKNOWLEDGMENTS

REFERENCES

[1] Walker, G., <u>Cryocoolers Part 1: Fundamentals</u>, Plenum Press, New York, 1983.

[2] Walker, G., <u>Cryocoolers Part 2: Applications</u>, Plenum Press, New York, 1983.

[3] Radebaugh, R., "Prospects for Small Cryocoolers," <u>Proceedings of the 9th International Cryogenics Engineering Conference</u>, May 1982, p. 761.

[4] Naes, L.G. and Nast, T.C., "Long Life Orbital Operation of Stirling Cycle Mechanical Refrigeration," <u>Proceedings of the 8th International Cryogenics Engineering Conference</u>. IPC Science and Technical Press, Surrey, England, 1980, pp. 204–212.

[5] Salomonovich, Sidyakina, Khaikin, Bakun, Nikonov, Maslakov, Klimenko, and Kurkin, "Space Helium Refrigerator," <u>Cryogenics</u>, August, IPC Business Press Ltd., 1981, pp. 474–478.

[6] Yasukochi, K., <u>Cryogenic Engineering</u>, (in Japanese), Vol. 13, 1978, pp. 257–271.

[7] Radebaugh, R., Zimmerman, J., Smith, D.R., and Louie, B., "A Comparison of Three Types of Pulse Tube Refrigerators: New Methods for Reaching 60 K." <u>Advances in Cryogenic Engineering</u>, Vol. 31, Plenum Press, New York, 1986, p. 1979.

[8] Rott, N., "Damped and Thermally Driven Acoustic Oscillations in Wide and Narrow Tubes," ZAMP, 20:230–243, 1969.

[9] Rott, N., "Thermally Driven Acoustic Oscillations, Part 2: Stability Limit for Helium," ZAMP, 24:54–72, 1973.

[10] (Lord) Rayleigh, "The Explanation of Certain Acoustical Phenomena," <u>Nature</u>, London, Volume 18, 1887, p. 319.

[11]   Gifford, W.E. and MacMahon, H.O., "A New Refrigeration Process," <u>Proceedings</u>
         <u>of the 10th International Congress of Refrigerations</u>, Copenhagen, Denmark,
         August 1959.

[12]   Gifford, W.E. and Longsworth, R.C., "Pulse–Tube Refrigeration," Transactions of
         the ASME, Vol. 63, 1964, p. 264.

[13]   Gifford, W.E. and Longsworth, R.C., "Pulse–Tube Refrigeration Progress,"
         <u>Advances in Cryogenic Engineering</u>, Vol. 10B, Plenum Press, New York, 1965, p.
         69.

[14]   Gifford, W.E. and Longsworth R.C., "Surface Heat Pumping," <u>Advances in</u>
         <u>Cryogenic Engineering</u>, Vol. 11, Plenum Press, New York, 1966, p. 171.

[15]   Longsworth, R.C., "An Experimental Investigation of PPulse Tube Refrigeration
         Heat Pumping Rates, " <u>Advances in Cryogenic Engineering</u>, Vol. 12, Plenum Press,
         New York, 1967, p 608

[16]   Gifford, W.E. and Kyanka, G.H., "Reversible Pulse Tube Refrigeration,"
         <u>Advances in Cryogenic Engineering</u>, Vol. 12, Plenum Press, New York, 1967, p. 619.

[17]   Merkli, P. and Thomann, H., "Thermoacoustic Effects in a Resonance Tube," <u>Fluid</u>
         <u>Mech</u>., Vol. 70, 1975, p. 161.

[18]   Wheatly, J., Hofler, T., Swift, G.W., and Migliori, A., "An Intrinsically
         Irreversible Thermoacoustic Heat Engine," <u>Acoustic Society of America</u>, Vol. 74,
         1983, p. 153.

[19]   Wheatley, J., Hofler, T., Swift, G.W., and Migliori, A., "Understanding Some
         Simple Phenomena in Thermoacouystics With Applications to Acoustical Heat
         Engineering," <u>American Journal of Physics</u>, Vol. 53, 1985, p. 147.

[20]   Mikulin, E.I., Shkrebyonock, M.P., and Tarasov, A.A., "Investigatiion of Cryogenic
         Pulse Tube," (in Russian) <u>Higher Educational Institutions News, Machinery</u>
         <u>Engineering</u>, 1:71 (1983)

[21]   Mikulin, E.I., Shkrebyonock, M.P., and Tarasov, A.A., "Expansion Cryogenic Pulse Tube," (in Russian) Higher Educational Institutions News, Machinery Engineering, 9:76 (1982)

[22]   Mikulin, E.I., Tarasov, A.A., and Shkrebyonock M.P., "Low Temperature Expansion Pulse Tubes," Advances in Cryogenic Engineering, Vol. 29, Plenum Press, New York, 1984, p. 629.

[23]   Herrmann , S. and Radebaugh R., "Measurements of the Efficiency and Refrigeration Power of Pulse–Tube Refrigeration," National Bureau of Standards Technical Note 1301, September 1986.

[24]   Radebaugh, R. and Herrmann, S., "Refrigeration Efficiency of Pulse Tube Refrigerators," Proceedings of the 4th International Cryocooler Conference, Boulder, Colorado, 1986.

[25]   Scott, R.E., "Notes on Linear Circuit Analysis," Northeastern University, Copyright 1956, Addison–Wesley.

[26]   Radebaugh, Ray, Chowdhury, K., Zimmerman, Jim, "Optimization of a Pulse Tube Refrigerator for a Fixed Compressor Swept Volume," Proceedings of the 5th International Cryocooler Conference, 1988.

APPENDIX A

DERIVATIONS

A.1   Derivation of $<\dot{m}_c>$: Flow Through Annular–Gap Isothermalizer

Assumptions: Ideal gas, laminar flow

$$dP/dx \ = \ f\,(\dot{m}/A_g)^2/2\rho r_h \tag{1}$$

$$f = \ 24/R_e \ = \ 24/(4r_h/\mu)(\dot{m}/A_g) \ = \ 6\mu/r_h(\dot{m}/A_g) \tag{2}$$

$$dP/dx \ = \ 3\mu\,(\dot{m}/A_g)/\rho r_h{}^2 \tag{3}$$

$$\dot{m} \ = \ (\rho r_h{}^2 A_g/3\mu)(dP/dx)$$

$$= \ (r_h{}^2 A_g/3\mu RT)P(dP/dx) \tag{4}$$

Integrate:

$$<\dot{m}> \ = \ (r_h{}^2 A_g/3\mu RT)\,(P_h{}^2 - P_l{}^2)/2L$$

$$= \ (r_h{}^2 A_g\rho/6\mu L)\,[(P_h/P_l) + 1]\,\Delta P \tag{5}$$

For Isothermalizer 2:

$r_h \ = \ t/2$ $t \ = \ $ annular gap thickness
$A_g \ = \ wt$ $w \ = \ $ annular gap width

Flow Impedance:

$$Z_f \ = \ 12L/wt^3 \tag{6}$$

$$<\dot{m}_c> \ = \ (\rho wt^3/24\mu L)\,[(P_h/P_l) + 1]\,\Delta P$$

$$<\dot{m}_c> \ = \ (\rho/2)\,[(P_h/P_l) + 1]\,(\Delta P/\mu Z_f) \tag{7}$$

A.2 Derivation of $<\dot{m}_h>$: Flow Through Orifice

Assumptions: Ideal gas, adiabatic flow, $(\Delta P/P) \ll 1$

$$<\dot{m}_h> \; = \; \Delta m/(\tau/2) \; = \; (2/\tau)(m_2 - m_1) \tag{1}$$

$$m_1 \; = \; P_1 V/RT_1 \tag{2}$$

$$m_2 \; = \; P_2 V/RT_2 \tag{3}$$

$$T_2 \; = \; T_1 \, (P_2/P_1)^{(\gamma-1)/\gamma} \tag{4}$$

$$m_2 = (V/RT_1) \, P_2 \, (P_2/P_1)^{(1-\gamma)/\gamma} \tag{5}$$

$$<\dot{m}_h> \; = \; (2/\tau) \, \frac{V}{RT_1} \, [P_2(P_2/P_1)^{1-\gamma/\gamma} - P_1] \tag{6}$$

$$= (2/\tau) \, \frac{P_1 V}{RT_1} \, [(P_2/P_1)^{1/\gamma} - 1] \tag{7}$$

$$= (2/\tau) \, \frac{P_1 V}{RT_1} \, [(\Delta P/P_1 + 1)^{1/\gamma} - 1] \tag{8}$$

Using a binomial expansion for small ΔP,

$$<\dot{m}_h> \; = \; (2/\tau) \, \frac{P_1 V}{RT_1} \, \left[\frac{1}{\gamma} \, \frac{\Delta P}{P_1} \right] \tag{9}$$

$$<\dot{m}_h> \; = \; (2/\tau) \, \frac{\Delta P V}{\gamma R T_1} \tag{10}$$

A.3 Mass Flow Rate Through Isothermalizer 2 for Turbulent Flow

Since flow rates with N_2 are so high, flow will not be laminar. Therefore, an expression for ΔP with the friction factor and the impedance factor Z_f must be found.

$$\Delta P = f \frac{L}{2\rho r_h} (\dot{m}/A_g)^2 \tag{1}$$

$$R_e = \frac{4r_h}{\mu} (\dot{m}/A_g) \tag{2}$$

$$\dot{m}/A_g = \frac{R_e \mu}{4 r_h} \tag{3}$$

$$\Delta P = f \frac{L \dot{m}}{2\rho_h \, A_g} \frac{R_e \mu}{4 r_h} = \frac{\dot{m} R_e \mu}{8\rho} \frac{L}{A_g r_h^2} \tag{4}$$

$$\Delta P = f \frac{\dot{m} R_e \mu}{2\rho} \frac{L}{w t^3} \tag{5}$$

$$Z_f = \frac{12 \, L}{w t^3} \tag{6}$$

$$\Delta P = f R_e \frac{\dot{m} \mu Z_f}{24\rho} \tag{7}$$

Trial and error procedure:

(1) Guess $\dot{m}$ (in turbulent region)

(2) Calculate Reynolds No., $R_e = \dfrac{4(\dot{m}/A_g) r_h}{\mu}$

(3) Find Fanning Friction Factor from Fig. 7–4 in Kays and London

(4) Calculate ΔP

$$\Delta P = f R_e = \frac{\dot{m} \mu Z_f}{24\rho}$$

$$Z_f = 6.870 \times 10^5 \text{ cm}^{-3}$$

$$\mu_{N_2} (10 \text{ atm, } 200 \text{ K}) = 132 \times 10^{-7} \text{ Pa} \cdot \text{s}$$

$$\rho_{N_2} \ (10 \text{ atm}, \ 200 \text{ K}) \ = \ .01721 \text{ g/cm}^3$$

(5) Compare experimental and calculated values of ΔP

(6) Adjust $\dot{m}$ accordingly and repeat

A.4 Calculation of Refrigeration Power Ratios for Table 3–1.

Experimental:

Constant (V_{cp}/V_t):

$$Q_{He}/Q_{N_2} \ = \ \frac{29.86}{14.74} \ = \ 2.026$$

Constant (P_d/P_a):

$$Q_{He}/Q_{N_2} \ = \ \frac{18.07}{14.74} \ = \ 1.226$$

Experimental Corrected:

Constant (V_{cp}/V_t):

$$\dot{Q}_{He}/\dot{Q}_{N_2} \ = \ (\dot{Q}_{He}/\dot{Q}_{N_2}) \ \frac{P_a \ N_2}{P_a \ He} \ \frac{V_{N_2}}{V_{He}} \ \frac{(\dot{m}_h/\dot{m}_c)_{N_2}}{(\dot{m}_h/\dot{m}_c)_{He}}$$

$$= \ (2.026) \ \left[\frac{1059}{1069}\right] \ \left[\frac{6.079}{6.070}\right] \ \left[\frac{0.181}{0.196}\right]$$

$$= \ 1.856$$

Constant (P_d / P_a):

$$(\dot{Q}_{He}/\dot{Q}_{N2}) = \frac{(\dot{m}_h/\dot{m}_c)_{N2}}{(\dot{m}_h/\dot{m}_c)_{He}} \frac{(P_d / P_a)^2_{N2}}{(P_d / P_a)^2_{He}}$$

$$= 0.848$$

Model:

Constant (V_{CP} / V_t):

$$Q_{He}/Q_{N2} = \gamma_{He}/\gamma_{N2} = \frac{1.67}{1.4} = 1.1929$$

Constant (P_d / P_a):

$$Q_{He}/Q_{N2} = \gamma_{He}/\gamma_{N2} = \frac{1.4}{1.67} = 0.8383$$

EXPERIMENTAL DATA

B.1   Experimental Data Showing Effect of Heat Transfer on
       Gross Refrigeration Power in OPTR

Tc (K)	Position of Temp. Probe (cm from hot end)	Gross Refrigeration (W)
149.9	0	19.95
150.0	6	19.54
149.9	13	17.83
199.5	0	32.61
200.0	3	30.36
200.0	6	29.15
200.0	10	28.67
199.9	13	27.19

B.2   Experimental Optimum Phase Angle

The following equation is developed from the phasor diagram in figure (2–4) and gives θ in terms of measureable quantities:

$$\text{Tan } \theta = \frac{<dM_t/dt>}{<\dot{m}_h>(T_h/T_c)} \tag{1}$$

$$<dM_t/dt> = \frac{P_d V_t}{\gamma R T_c} \omega . \tag{2}$$

Experimental Data for Calculation of Optimum Phase Angle

Data Set No.	T_c (K)	$\langle \dot{M}h \rangle$ (g/s)	$\langle dM_t/dt \rangle$ (g/s)	Θ (deg)
1	82.0	0.0817	0.150	40.2
	79.9	0.1225	0.3240	29.1
	95.2	0.1943	0.2452	17.8
2	122.4	0.1334	0.2746	33.9
	126.4	0.1772	0.2427	24.8
	134.4	0.2119	0.2170	20.2
	151.3	0.2688	0.1814	15.2
3	146.5	0.0803	0.2561	51.2
	130.8	0.1242	0.2440	34.4
	128.0	0.1517	0.2240	26.7
	129.3	0.1791	0.2060	21.6
4	90.4	0.0971	0.3918	44.2
	71.6	0.1124	0.4066	34.6
	78.1	0.1640	0.3084	21.4
5	98.5	0.0505	0.2752	55.0
	74.0	0.0869	0.2681	31.3
	87.3	0.1404	0.2140	19.5
	131.3	0.2140	0.1591	14.6
6	153.9	0.0999	0.3122	52.0
	135.3	0.1367	0.3005	38.4
	125.4	0.1529	0.2853	32.0
	122.4	0.1686	0.2657	27.2

B.3 Experimental and Theoretical Data

T_c (K)	Freq (Hz)	P_a (kP$_a$)	P_d/P_a	$\dot{M}_c$ (g/s)	$\dot{M}_h/\dot{M}_c$	T_h/T_c
110.0	6.098	1198	0.307	2.579	0.132	2.909
150.0	6.061	1016	0.355	1.731	0.184	2.167
150.0	6.098	1206	0.350	2.344	0.157	2.167
150.0	6.135	779	0.337	1.053	0.227	2.167
150.0	6.061	575	0.262	0.636	0.250	2.167
150.0	6.061	1205	0.348	2.328	0.160	2.167
150.0	6.061	1200	0.351	2.256	0.172	2.167
189.0	6.135	1236	0.387	2.288	0.181	1.799
200.0	6.098	1072	0.388	1.924	0.199	1.700
200.0	6.098	1039	0.330	1.365	0.223	1.700
200.0	6.024	1071	0.201	0.734	0.330	1.700
200.0	6.098	1072	0.323	1.452	0.335	1.700
200.0	6.098	1025	0.292	1.115	0.300	1.700
200.0	6.098	1057	0.321	1.855	0.203	1.700
200.0	6.061	1076	0.388	1.883	0.184	1.700
200.0	6.061	1085	0.388	1.424	0.327	1.700
200.0	6.024	1089	0.325	1.905	0.248	1.700
84.9	5.98	1252	0.290	4.4	0.11	3.651
85.0	6.02	1245	0.301	4.190	0.095	3.647
95.6	5.98	1204	0.307	3.44	0.16	3.295
95.5	6.06	1188	0.319	3.200	0.126	3.298
120.0	6.06	1146	0.346	2.170	0.220	2.667
119.8	6.02	1135	0.364	2.000	0.148	2.671
119.5	6.06	1156	0.336	2.34	0.23	2.678
151.1	5.95	1247	0.367	2.05	0.29	2.151
151.1	5.05	1250	0.379	1.970	0.240	2.151
188.5	5.88	1222	0.385	1.3	0.54	1.804
187.2	5.85	1223	0.396	1.250	0.460	1.790
187.5	5.95	1225	0.410	1.170	0.280	1.787
209.8	5.95	1155	0.397	1.25	0.53	1.668
234.7	6.02	1221	0.420	1.090	0.490	1.534
234.7	6.02	1220	0.445	1.090	0.280	1.532
235.7	6.09	1218	0.409	1.07	0.58	1.527
274.1	6.02	1211	0.421	1.03	0.66	1.368
273.6	6.13	1213	0.433	1.020	0.530	1.371
275.0	6.06	1215	0.440	0.942	0.410	1.364
275.1	6.09	1217	0.460	0.905	0.230	1.363

B.3 Experimental and Theoretical Data (Continued)

EXP q_r/RT_c (J/g)	Model 1 $2<\dot{H}>/\dot{m}_cRT$	Th/Exp Ratio	Exp $\dot{Q}_{gross}$ (W)	Model 2 $<\dot{H}>$ (W)	Model 3 $<\dot{H}>$ (W)	Th/Exp Ratio 2	Th/Ex Ratio
0.0337	0.1852	5.49	9.94	134.86	65.29	13.57	6.57
0.0686	0.2223	3.24	18.51	183.23	74.85	9.90	4.04
0.0546	0.1870	3.43	19.95	184.09	73.64	9.23	3.69
0.0816	0.2604	3.19	13.40	166.54	71.01	12.43	5.30
0.0666	0.2229	3.35	6.60	103.99	45.62	15.76	6.91
0.0551	0.1895	3.44	20.01	185.25	74.26	9.26	3.71
0.0573	0.2055	3.59	20.15	200.02	80.91	9.93	4.02
0.0635	0.1979	3.12	28.54	241.96	83.14	8.48	2.91
0.0852	0.2062	2.42	34.08	229.92	76.39	6.75	2.24
0.0713	0.1965	2.76	20.23	212.39	71.62	10.50	3.54
0.0649	0.1820	2.80	9.9	200.26	75.27	20.23	7.60
0.1080	0.2889	2.67	32.61	322.22	120.50	9.88	3.70
0.0770	0.2339	3.04	17.84	249.42	89.68	13.98	5.03
0.0845	0.1740	2.06	32.60	191.33	63.71	5.87	1.95
0.0703	0.1906	2.71	27.54	212.09	69.88	7.70	2.54
0.0938	0.3388	3.61	27.76	380.08	140.77	13.69	5.07
0.0707	0.2152	3.04	28.00	240.86	82.69	8.60	2.95
0.0297	0.1830	6.17	11.52	108.80	60.18	9.44	5.22
0.0325	0.1638	5.04	12.03	97.63	53.08	8.12	4.41
0.0374	0.2542	6.79	12.80	161.10	88.87	12.59	6.94
0.0433	0.2083	4.81	13.84	131.82	69.32	9.52	5.01
0.0658	0.3189	4.85	17.80	240.81	122.98	13.52	6.91
0.0483	0.2260	4.68	12.03	167.68	77.86	13.94	6.47
0.0578	0.3251	5.62	16.80	246.61	128.78	14.68	7.67
0.0875	0.3596	4.11	28.17	359.72	166.54	12.77	5.91
0.0865	0.3073	3.55	26.78	308.17	132.60	11.51	4.95
0.1253	0.5890	4.70	31.92	680.49	569.65	21.32	17.85
0.1132	0.5121	4.52	27.53	593.68	310.54	21.56	11.28
0.0715	0.3222	4.51	16.30	381.17	142.16	23.38	8.72
0.1249	0.5514	4.42	34.04	658.69	371.90	19.35	10.93
0.1400	0.4959	3.54	37.22	689.09	279.74	18.51	7.52
0.0919	0.2998	3.26	23.13	416.86	128.50	18.02	5.56
0.1591	0.5691	3.58	41.70	801.56	427.01	19.22	10.24
0.1587	0.5971	3.76	46.57	922.75	476.58	19.81	10.23
0.1472	0.4941	3.36	42.70	777.33	274.66	18.20	6.43
0.1059	0.3864	3.65	28.53	605.07	180.11	21.21	6.31
0.0680	0.2265	3.33	17.61	357.20	93.80	20.28	5.33

4. TITLE AND SUBTITLE

Analytical Model for the Refrigeration Power of the Orifice Pulse Tube Refrigerator

5. AUTHOR(S)

Peter J. Storch, Ray Radebaugh, and James E. Zimmerman

11. ABSTRACT (A 200-WORD OR LESS FACTUAL SUMMARY OF MOST SIGNIFICANT INFORMATION. IF DOCUMENT INCLUDES A SIGNIFICANT BIBLIOGRAPHY OR LITERATURE SURVEY, MENTION IT HERE.)

The pulse tube refrigerator is a cryocooler with potential for high reliability. This regenerative refrigerator operates with low average pressures, small compression ratios, and only one moving part. In research conducted at the National Institute of Standards and Technology, a pulse tube refrigerator with an orifice located at the closed, hot end of the system has been used to reach 60 K in one stage. A gross refrigeration power of 12 W has been measured at 80 K with a pulse tube volume of 30 cm^3. This paper presents the development of an analytical model to predict the refrigeration power produced in an orifice pulse tube. Three versions of the model are presented: the first calculates quantities which are independent of dead volume; the second neglects dead volume; and the third describes a system with dead volume. Experimental results confirm predictions by the model that refrigeration power is proportional to the average pressure, the pulse frequency, the mass flow ratio, and the square of the dynamic pressure ratio. Results are presented that are useful for approximate design of orifice pulse tube systems. The model assumes adiabatic conditions and an energy balance is performed in terms of net enthalpy flow. Phasor analysis was found to be very useful for analyzing the oscillations of pressure, temperature, and mass flow rate.

12. KEY WORDS (6 TO 12 ENTRIES; ALPHABETICAL ORDER; CAPITALIZE ONLY PROPER NAMES; AND SEPARATE KEY WORDS BY SEMICOLONS)

analytical model; cryocooler; cryogenics; pulse tube refrigerator; refrigeration power, refrigerator

13. AVAILABILITY

X	UNLIMITED
	FOR OFFICIAL DISTRIBUTION. DO NOT RELEASE TO NATIONAL TECHNICAL INFORMATION SERVICE (NTIS).
X	ORDER FROM SUPERINTENDENT OF DOCUMENTS, U.S. GOVERNMENT PRINTING OFFICE, WASHINGTON, DC 20402.
	ORDER FROM NATIONAL TECHNICAL INFORMATION SERVICE (NTIS), SPRINGFIELD, VA 22161.

14. NUMBER OF PRINTED PAGES

94

15. PRICE

ELECTRONIC FORM

NIST Technical Publications

Periodical

Journal of Research of the National Institute of Standards and Technology—Reports NIST research and development in those disciplines of the physical and engineering sciences in which the Institute is active. These include physics, chemistry, engineering, mathematics, and computer sciences. Papers cover a broad range of subjects, with major emphasis on measurement methodology and the basic technology underlying standardization. Also included from time to time are survey articles on topics closely related to the Institute's technical and scientific programs. Issued six times a year.

Nonperiodicals

Monographs—Major contributions to the technical literature on various subjects related to the Institute's scientific and technical activities.

Handbooks—Recommended codes of engineering and industrial practice (including safety codes) developed in cooperation with interested industries, professional organizations, and regulatory bodies.

Special Publications—Include proceedings of conferences sponsored by NIST, NIST annual reports, and other special publications appropriate to this grouping such as wall charts, pocket cards, and bibliographies.

Applied Mathematics Series—Mathematical tables, manuals, and studies of special interest to physicists, engineers, chemists, biologists, mathematicians, computer programmers, and others engaged in scientific and technical work.

National Standard Reference Data Series—Provides quantitative data on the physical and chemical properties of materials, compiled from the world's literature and critically evaluated. Developed under a worldwide program coordinated by NIST under the authority of the National Standard Data Act (Public Law 90-396). NOTE: The Journal of Physical and Chemical Reference Data (JPCRD) is published quarterly for NIST by the American Chemical Society (ACS) and the American Institute of Physics (AIP). Subscriptions, reprints, and supplements are available from ACS, 1155 Sixteenth St., NW., Washington, DC 20056.

Building Science Series—Disseminates technical information developed at the Institute on building materials, components, systems, and whole structures. The series presents research results, test methods, and performance criteria related to the structural and environmental functions and the durability and safety characteristics of building elements and systems.

Technical Notes—Studies or reports which are complete in themselves but restrictive in their treatment of a subject. Analogous to monographs but not so comprehensive in scope or definitive in treatment of the subject area. Often serve as a vehicle for final reports of work performed at NIST under the sponsorship of other government agencies.

Voluntary Product Standards—Developed under procedures published by the Department of Commerce in Part 10, Title 15, of the Code of Federal Regulations. The standards establish nationally recognized requirements for products, and provide all concerned interests with a basis for common understanding of the characteristics of the products. NIST administers this program as a supplement to the activities of the private sector standardizing organizations.

Consumer Information Series—Practical information, based on NIST research and experience, covering areas of interest to the consumer. Easily understandable language and illustrations provide useful background knowledge for shopping in today's technological marketplace.

Order the above NIST publications from: Superintendent of Documents, Government Printing Office, Washington, DC 20402.

Order the following NIST publications—FIPS and NISTIRs—from the National Technical Information Service, Springfield, VA 22161.

Federal Information Processing Standards Publications (FIPS PUB)—Publications in this series collectively constitute the Federal Information Processing Standards Register. The Register serves as the official source of information in the Federal Government regarding standards issued by NIST pursuant to the Federal Property and Administrative Services Act of 1949 as amended, Public Law 89-306 (79 Stat. 1127), and as implemented by Executive Order 11717 (38 FR 12315, dated May 11, 1973) and Part 6 of Title 15 CFR (Code of Federal Regulations).

NIST Interagency Reports (NISTIR)—A special series of interim or final reports on work performed by NIST for outside sponsors (both government and non-government). In general, initial distribution is handled by the sponsor; public distribution is by the National Technical Information Service, Springfield, VA 22161, in paper copy or microfiche form.